

# Super-Beamforming in Holographic MIMO

Andrea Pizzo<sup>1\*</sup> and Angel Lozano<sup>1</sup>

<sup>1</sup>Department of Engineering, Univ. Pompeu Fabra, Barcelona 08005, Spain.

\*Corresponding author(s). E-mail(s): [andrea.pizzo@upf.edu](mailto:andrea.pizzo@upf.edu);

Contributing authors: [angel.lozano@upf.edu](mailto:angel.lozano@upf.edu);

## Abstract

The conventional linear scaling of beamforming gain with the number of antennas is not a fundamental physical limitation, but rather a consequence of the half-wavelength spacings that minimize mutual coupling. Relaxing this constraint facilitates beamforming gains exceeding those of uncoupled arrays along specific directions. This paper shows that, when antenna losses remain sufficiently small, mutual coupling enables the synthesis of *superbeams* whose endfire gain scales quadratically with the number of antennas. Notably, this quadratic scaling does not necessarily require vanishing spacings, but emerges for spacings slightly below half wavelength as the array aperture increases.

**Keywords:** Holographic MIMO, supergain, superdirectivity, mutual coupling, spatial sampling theorem, spectral concentration.

## 1 Introduction

Arranging  $N$  isotropic antennas into a uniform linear array (ULA) can increase the gain by a factor of  $N$  relative to a single antenna [1, Sec. 6]. This linear scaling, however, is not a fundamental limit, but rather a consequence of the half-wavelength antenna spacing typically adopted to ensure that the excitation currents are as they would be for the antennas in isolation (without mutual coupling). Reducing the spacing below this threshold leads to a holographic array, where currents become inherently coupled and the assumption of independence is superseded [2, 3]. Far from being a mere parasitic effect, coupling can be harnessed to synthesized radiation patterns that exceed the gain of half-wavelength-spaced ULAs for the same number of antennas, a phenomenon aptly named supergain (or superdirectivity) [4–6].

Supergain is classically associated with a vanishing antenna spacing, with correspondingly small apertures and maximal mutual coupling. In this regime, the endfire (aligned to the array axis) gain approaches a quadratic scaling with  $N$  [7]. Such behavior is often dismissed

as impractical; it requires precise current distributions that are hypersensitive to structural perturbations and are accompanied by surges in the reactive-to-radiated power ratio, characterized by a high array quality ( $Q$ ) factor [6, 8]. High- $Q$  arrays are inherently constrained to a narrow operational bandwidth near resonance, and their resonant frequencies cannot be adjusted without structural re-tuning [9, 10]. Furthermore, achieving the requisite  $Q$ -factors demands delicate engineering and calibration, often at the expense of other design objectives.

Despite these intrinsic challenges, there has been a significant resurgence of interest in supergain [11–15] and related effects [16, 17], driven by the quest for extreme array gains with compact apertures. These efforts are driven by recent developments in reconfigurable metasurfaces that may enable ultra-high  $Q$ -factors at arbitrary, easily tunable resonant frequencies [18, 19]. Realizability is further enhanced by intrinsic antenna losses, which give rise to a trade-off between achievable gain and physical sensitivity of the array [12, 20].

Building on these advances, this paper establishes a comprehensive framework for the analysis and design of supergain arrays. This framework generalizes the classical regime of electrically small apertures to account for antenna losses. In addition, the framework reveals another supergain regime in which coupling builds up from the accrual of contributions from a large number of antennas that, having non-vanishing spacings, are only partially coupled. The specific contributions are as follows:

- The physical limitations imposed by dissipative losses on supergain are characterized, extending classical lossless analyses for electrically small apertures [7]. A rigorous asymptotic analysis as the antenna spacing vanishes reveals the interplay between the number of antennas and the loss factor, formalizing previous numerical observations [12, 21].
- A novel supergain regime is identified, that emerges as the array aperture widens while the antenna spacing remains fixed somewhere below the half-wavelength mark. This rigorously establishes the qualitative behavior predicted in [22], demonstrating its physical accessibility in wide-aperture holographic arrays.

The manuscript is organized as follows. Section 2 reviews the discrete-space Fourier transform for ULAs, establishing the array gain and quality factor. Section 3 characterizes how mutual coupling impacts array performance measures, and Section 4 examines the physical limits under strong coupling. Section 5 provides a rigorous framework based on spectral concentration theory, and Section 6 specializes this theory to the spatial domain for ULAs. Building on this, Sections 7 and 8 formalize the array behavior in limiting regimes. Section 9 concludes with a discussion on potential extensions.

*Notation:* The Hilbert-Schmidt space of square-integrable complex functions over  $\mathcal{X}$  is denoted by  $\mathcal{L}^2(\mathcal{X})$ , with inner product  $\langle f, g \rangle = \int_{\mathcal{X}} f(x)g^*(x) dx$  and norm  $\|f\| = \sqrt{\langle f, f \rangle}$ . For periodic functions, the  $\mathcal{L}^2$ -norm is computed over the main period unless otherwise stated. Landau symbols are employed, namely  $f(x) = \mathcal{O}(g(x))$  indicates that  $|f(x)/g(x)|$  is bounded above by a constant,  $f(x) = o(g(x))$  indicates that  $f(x)$  grows strictly more slowly than  $g(x)$ , and  $f(x) \sim g(x)$  indicates that  $f(x)/g(x) \rightarrow 1$ . In turn,  $\text{sinc}(x) = \sin(\pi x)/\pi x$  and  $[x]_{\text{rem } 2\pi} = x - 2\pi \lfloor x/2\pi \rfloor$  is the remainder of  $x$  modulo  $2\pi$

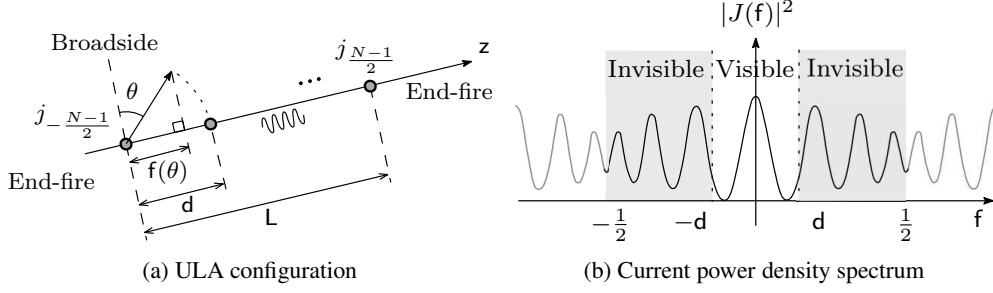


**Fig. 1:** (a) Geometry of a linear array of  $N$  punctiform antennas spaced by a normalized distance  $d$  and aligned with the  $z$ -axis; the array's aperture is  $L = (N - 1)d$ . The direction of propagation forms an angle  $\theta$  with respect to the array's normal. The  $n$ th antenna is excited by a complex-valued current weight  $j_n$ . (b) Periodic power density spectrum of the current vs the discrete spatial frequency,  $f$ . The main period splits into a visible and an invisible region.

## 2 Uniform Linear Arrays

All spatial variables are normalized by the wavelength, and they are therefore dimensionless. A time-harmonic and single polarization setting is considered, whereby electromagnetic quantities can be expressed as complex scalars.

### 2.1 Space-Time Isomorphism

Consider a  $z$ -aligned uniform array of  $N$  punctiform (isotropic) antennas spaced by a normalized distance  $d > 0$ , spanning an aperture of normalized length  $L = (N - 1)d$  (see Fig. 1). The array is referenced to its midpoint, and the antenna indices are given by the index set

$$[N] = \left\{ -\frac{N-1}{2}, \dots, \frac{N-1}{2} \right\} \quad (1)$$

for odd  $N$ . The array is driven by a current vector  $\mathbf{j} = \{j_n\} \in \mathcal{L}^2([N])$ , where each entry  $j_n$  is the phasor of the current driving the  $n$ th antenna. The discrete-space Fourier transform of  $\mathbf{j}$  yields the current spectrum

$$J(f) = F \mathbf{j} = \sum_{n \in [N]} j_n e^{-j2\pi f n}, \quad (2)$$

with corresponding inverse Fourier transform (in the energy sense)

$$j_n = F^{-1} J(f) = \int_{-1/2}^{1/2} J(f) e^{j2\pi f n} df \quad n \in [N], \quad (3)$$

where  $F$  and  $F^{-1}$  are the unitary forward and inverse Fourier transform operators, respectively. The current spectrum  $J(f)$ , periodic with period 1, belongs to the space of square-integrable functions  $\mathcal{L}^2[-\frac{1}{2}, \frac{1}{2}]$ . It corresponds to the far-field radiation pattern as a function

of direction, which is encoded through the normalized spatial frequency

$$f(\theta) = d \sin \theta = d f(\theta), \quad (4)$$

where  $\theta \in [-\frac{\pi}{2}, \frac{\pi}{2}]$  is the angle relative to broadside, and  $f(\theta) = \sin \theta$  is the spatial frequency (see Fig. 1). Physically,  $f(\theta)$  is the frequency along an asymptotically long continuous aperture of the current that must be excited to radiate a plane wave  $e^{j2\pi f(\theta)z}$  on direction  $\theta$ . Then,  $f(\theta)$  results from sampling that aperture with isotropic antennas spaced by  $d$ . Low spatial frequencies correspond to near-broadside propagation ( $\theta \approx 0$ ) whereas high spatial frequencies map to near-endfire directions ( $|\theta| \approx \pi/2$ ).

As  $\theta$  varies over its domain, the mapping  $\theta \mapsto f$  confines  $f$  to the so-called *visible region*,  $[-d, d]$ , corresponding to directions associated with propagating waves (see Fig. 1b). Plane waves with spatial frequencies within this region carry real power, contributing to the radiation. In contrast, plane waves with spatial frequencies obtained by analytic continuation into the invisible region  $|f| > d$  are evanescent and store reactive (imaginary) power, which oscillates without producing net radiation [23, 24]. To prevent spatial aliasing, it must hold that  $d \leq 1/2$ ; otherwise, grating lobes would appear within the visible region.

## 2.2 Performance Measures

The *directivity function* in a certain direction specified by  $f$  via (4) is defined as the ratio of the power density radiated at  $f$  to the average radiated power across all visible directions

$$D(N, d, \mathbf{j}, f) = G(N, d, 0, \mathbf{j}, f) = \frac{|J(f)|^2}{\frac{1}{2d} \int_{-d}^d |J(\mathbf{g})|^2 d\mathbf{g}}. \quad (5)$$

By construction, averaging (5) over the visible region returns 1. Thus, the directivity quantifies how effectively the array concentrates power along a specific direction relative to an isotropic radiator. This isotropic reference corresponds to  $N = 1$ , where the array collapses into a single punctiform antenna producing spherical wavefronts. In practice, current weights are applied to the array by signal generators through an impedance network, but the array gain is independent of such circuitry details [12] and the impedance network is therefore omitted.

The introduction of losses via the factor  $\rho = R_L/R_R \geq 0$ , with  $R_R$  and  $R_L$  the radiation resistance and loss resistance, yields the *array gain function* at  $f$  [1, Sec. 2.9], [25]

$$G(N, d, \rho, \mathbf{j}, f) = \frac{|J(f)|^2}{\frac{1}{2d} \int_{-d}^d |J(\mathbf{g})|^2 d\mathbf{g} + \rho \int_{-1/2}^{1/2} |J(\mathbf{g})|^2 d\mathbf{g}} \quad (6)$$

which subsumes (5) for  $\rho = 0$ , corresponding to lossless antennas. The loss factor  $\rho$  relates to the antenna radiation efficiency  $0 \leq \eta \leq 1$  via

$$\eta(\rho) = \frac{1}{1 + \rho} = \frac{R_R}{R_R + R_L}. \quad (7)$$

Let us also formalize the definition of the  $Q$  factor as the ratio of the power radiated and stored in the fields excited by the antennas to the average power accepted by them [6, 25–27]

$$Q(N, \mathbf{d}, \rho, \mathbf{j}) = \frac{\int_{-1/2}^{1/2} |J(\mathbf{g})|^2 d\mathbf{g}}{\frac{1}{2d} \int_{-\mathbf{d}}^{\mathbf{d}} |J(\mathbf{g})|^2 d\mathbf{g} + \rho \int_{-1/2}^{1/2} |J(\mathbf{g})|^2 d\mathbf{g}}. \quad (8)$$

The  $Q$  factor plays a central role in the design of arrays. Each array can be modeled as a resonant circuit that supports currents at temporal frequencies (in Hz) close to resonance [6, 9, 10]. The reciprocal of  $Q$  is proportional to the ratio of the resonance bandwidth  $\Delta_f$  to the resonant frequency  $f_0$ ,

$$\frac{1}{Q} \propto \frac{\Delta_f}{f_0}, \quad (9)$$

which measures the sharpness of the resonance. The lower  $Q$ , the wider the bandwidth. (The circuit-based model is accurate only for moderately high  $Q$ , becoming unreliable for  $Q < 2$ .)

### 2.3 Normalization

Taking advantage of the scale invariances of (6) and (8), both the current vector  $\mathbf{j}$  and its transform  $J(\mathbf{f})$  can be normalized to have unit  $\mathcal{L}^2$ -norms irrespective of  $N$ , namely

$$\|\mathbf{j}\|^2 = \|J\|^2 = 1, \quad (10)$$

as per Parseval's theorem. This ensures that the total (radiated and stored) power is fixed across all current distributions, isolating the effect of beamforming through changes in that distribution. Under this normalization, the array gain in (6) becomes

$$G(N, \mathbf{d}, \rho, \mathbf{j}, \mathbf{f}) = \frac{|J(\mathbf{f})|^2}{\frac{1}{2d} \int_{-\mathbf{d}}^{\mathbf{d}} |J(\mathbf{g})|^2 d\mathbf{g} + \rho} \quad (11)$$

and the  $Q$  factor in (8) satisfies

$$Q^{-1}(N, \mathbf{d}, \rho, \mathbf{j}) = \frac{1}{2d} \int_{-\mathbf{d}}^{\mathbf{d}} |J(\mathbf{g})|^2 d\mathbf{g} + \rho. \quad (12)$$

### 2.4 Optimality Criterion

The optimality of the introduced performance measures is governed by their common term, the average radiated power

$$\frac{1}{2d} \int_{-\mathbf{d}}^{\mathbf{d}} |J(\mathbf{g})|^2 d\mathbf{g}. \quad (13)$$

There is a tension in that maximizing the array gain entails decreasing the power within the visible region, whereas minimizing the  $Q$  factor entails the opposite. The ensuing tradeoff

embodies the fundamental tension between array gain and usable bandwidth [6, 9]. Additionally, antenna losses act through  $\rho$  as a Tikhonov-type physical regularization. Increasing  $\rho$  diminishes the impact of (13) on performance measures, expanding the usable bandwidth but taking a toll on gain. Another tradeoff thus arises between maximum gain, for  $\rho = 0$ , and physical realizability, corresponding to  $\rho > 0$  and a surging dissipated power.

In the sequel, the optimality criterion is set to be the maximization of the array gain, while the  $Q$  factor is evaluated to quantify the corresponding bandwidth cost. Optimizations for minimal  $Q$  factor or mixed strategies are also possible [26–28]. The superscript  $*$  denotes quantities evaluated for the current vector that maximizes the array gain. For instance, the current  $\mathbf{j}^*(\mathbf{d}, \rho, \mathbf{f}')$  that maximizes the gain at a given beamforming direction  $\mathbf{f}'$  satisfies

$$\underset{\mathbf{j}: \|\mathbf{j}\|=1}{\text{maximize}} G(N, \mathbf{d}, \rho, \mathbf{j}, \mathbf{f}'), \quad (14)$$

with spectrum  $J^*(\mathbf{d}, \rho, \mathbf{f}', \mathbf{f})$  defined according to (2). For the above current, the array gain in the beamforming direction  $\mathbf{f}'$  is  $G^*(N, \mathbf{d}, \rho, \mathbf{f}') = G(N, \mathbf{d}, \rho, \mathbf{j}^*, \mathbf{f}')$  while the  $Q$  factor equals  $Q^*(N, \mathbf{d}, \rho, \mathbf{f}') = Q(N, \mathbf{d}, \rho, \mathbf{j}^*)$ .

### 3 Spatial Coupling

#### 3.1 Uncoupled Arrays

Consider a fixed spacing  $d = 1/2$ . Isotropic antennas then act as independent transducers, with an overall array response equal to the sum of the individual antenna contributions [29]. From (12), the  $Q$  factor with such half-wavelength spacing reduces to the antenna efficiency in (7), regardless of the current vector,

$$Q(N, \frac{1}{2}, \rho, \mathbf{j}) = \eta(\rho). \quad (15)$$

As of the array gain, by expanding  $J(\mathbf{f})$  in the numerator of (11) according to (2), and in light of the normalization in (10), it reduces to

$$G(N, \frac{1}{2}, \rho, \mathbf{j}, \mathbf{f}) = N \eta(\rho) |\mathbf{a}(\mathbf{f})^H \mathbf{j}|^2 \quad (16)$$

where

$$\mathbf{a}(\mathbf{f}) = \frac{1}{\sqrt{N}} \left( e^{-j\pi\mathbf{f}(N-1)}, \dots, e^{j\pi\mathbf{f}(N-1)} \right)^T \quad (17)$$

is the array response vector, satisfying  $\|\mathbf{a}\| = 1$ . In this case, beamforming via maximum-ratio transmission is optimal for any direction defined by  $\mathbf{f}'$ . Indeed, from the Cauchy–Schwarz inequality applied to (16),

$$\mathbf{j}^*(\frac{1}{2}, \rho, \mathbf{f}') = \mathbf{a}(\mathbf{f}'), \quad (18)$$

yielding

$$G^*(N, \frac{1}{2}, \rho, \mathbf{f}') = N \eta(\rho). \quad (19)$$

From (2), the spectrum corresponding to (18) is

$$J^*(\frac{1}{2}, \rho, f', f) = \frac{D_N(f - f')}{\sqrt{N}}, \quad (20)$$

where  $D_N(f)$  is the  $N$ th order Dirichlet kernel

$$D_N(f) = \sum_{n \in [N]} e^{-j2\pi fn} = \frac{\sin(\pi Nf)}{\sin(\pi f)}. \quad (21)$$

This kernel is real-symmetric and positive-definite, attaining its maximum at the origin, where it equals  $D_N(0) = N$  [1, Ch. 6]. From Parseval's theorem, and consistently with (10), its energy is

$$\int_{-1/2}^{1/2} D_N^2(f) df = N. \quad (22)$$

### 3.2 Impact of Coupling

The uniformity in array gain breaks down for  $d < 1/2$  due to a surge in antenna interactions. Expanding  $J(f)$  in (6) according to (2) while evaluating the integral

$$\int_{-d}^d e^{j2\pi fn} df = \frac{\sin(2\pi dn)}{\pi n}, \quad (23)$$

what emerges is the generalized Rayleigh quotient [6, 26]

$$G(N, d, \rho, \mathbf{j}, f) = N \frac{|\mathbf{a}(f)^H \mathbf{j}|^2}{\mathbf{j}^H \mathbf{C}(d, \rho) \mathbf{j}} \quad (24)$$

with  $\mathbf{a}(f)$  as defined in (17) while  $\mathbf{C} \in \mathbb{R}^{N \times N}$  denotes the lossy coupling matrix [12, 20]

$$\mathbf{C}(d, \rho) = \mathbf{C}(d) + \rho \mathbf{I}_N. \quad (25)$$

The matrix  $\mathbf{C}(d)$  represents the coupling in the lossless case. It is real, symmetric, Toeplitz, and positive-definite, its entries given by

$$[\mathbf{C}(d)]_{n,m} = \frac{\sin(2\pi d(n-m))}{2\pi d(n-m)} \quad n, m = 0, \dots, N-1 \quad (26)$$

specifying, up to a scaling factor, the power radiated by the  $n$ th antenna and captured by its  $m$ th counterpart [12]. The off-diagonal entries thus quantify the mutual coupling between distinct array antennas. Let the ordered eigenvalues of  $\mathbf{C}$  be  $\lambda_0(N, d) > \dots > \lambda_{N-1}(N, d) > 0$  with eigenvectors  $\mathbf{v}_0(N, d), \dots, \mathbf{v}_{N-1}(N, d)$ . The affine transformation in (25) does not alter the eigenvectors, while the eigenvalues of the lossy coupling matrix  $\mathbf{C}$  become

$$\lambda_k(N, d, \rho) = \lambda_k(N, d) + \rho. \quad (27)$$

The lossy coupling matrix  $\mathbf{C}$  retains the structure of its lossless brethren and satisfies  $\text{tr}(\mathbf{C}) = N(1 + \rho)$ . For  $d = 1/2$ , the coupling matrix reduces to identity, confirming that mutual coupling vanishes in uniform linear arrays under this configuration [12].

The  $Q$  factor in (12), in turn, can be obtained as [6, 26]

$$Q(N, d, \rho, \mathbf{j}) = (\mathbf{j}^H \mathbf{C}(d, \rho) \mathbf{j})^{-1}. \quad (28)$$

## 4 Supergain

### 4.1 Supergain Characterization

To isolate the effect of coupling, arising from having  $d < 1/2$ , from the effects of changing the current distribution, the maximum array gain  $G^*(N, d, \rho, f')$  in (24) is normalized by its uncoupled, lossless counterpart  $G^*(N, \frac{1}{2}, 0, f')$  in (19). This ratio defines the *supergain* factor

$$G^*(N, d, \rho, f') = \frac{G^*(N, d, \rho, f')}{G^*(N, \frac{1}{2}, 0, f')}. \quad (29)$$

In the lossless case (i.e., for  $\rho = 0$ ),  $G^*$  specializes to

$$D^*(N, d, f') = G^*(N, d, 0, f'). \quad (30)$$

We further distinguish between the broadside ( $G_{\perp}^*$ ,  $D_{\perp}^*$ ) and endfire ( $G_{\parallel}^*$ ,  $D_{\parallel}^*$ ) cases, corresponding to currents optimized for beamforming directions perpendicular and parallel to the linear array axis, respectively (see Fig. 1).

Substituting (24) into (29), the optimal current for any  $f'$  is returned by

$$\underset{\mathbf{j}: \|\mathbf{j}\|=1}{\text{maximize}} \frac{\mathbf{j}^H \mathbf{A}(f') \mathbf{j}}{\mathbf{j}^H \mathbf{C}(d, \rho) \mathbf{j}}, \quad (31)$$

where  $\mathbf{C}$  is the coupling matrix in (25) while  $\mathbf{A} = \mathbf{a}\mathbf{a}^H$ , recalling that  $\mathbf{a}$  is the array response vector in (17). Because the problem is unaffected by scalings, the constraint  $\|\mathbf{j}\| = 1$  is momentarily dropped and  $\mathbf{j}$  is normalized such that the denominator is unity, i.e.,

$$\begin{aligned} & \underset{\mathbf{j}}{\text{maximize}} \quad \mathbf{j}^H \mathbf{A}(f') \mathbf{j} \\ & \text{subject to} \quad \mathbf{j}^H \mathbf{C}(d, \rho) \mathbf{j} = 1. \end{aligned} \quad (32)$$

The KKT conditions yield the generalized eigenvalue problem

$$\mathbf{A}(f') \mathbf{j}^* = \lambda^* \mathbf{C}(d, \rho) \mathbf{j}^* \quad (\mathbf{j}^*)^H \mathbf{C}(d, \rho) \mathbf{j}^* = 1. \quad (33)$$

Since  $\mathbf{A}(f')$  is of unit rank, the generalized eigenvector  $\mathbf{j}^* \in \text{span}(\mathbf{C}^{-1} \mathbf{a})$  is the unique (up to a factor) maximizer. Reintroducing the normalization condition in (10),

$$\mathbf{j}^*(d, \rho, f') = \frac{\mathbf{C}(d, \rho)^{-1} \mathbf{a}(f')}{\|\mathbf{C}(d, \rho)^{-1} \mathbf{a}(f')\|}. \quad (34)$$

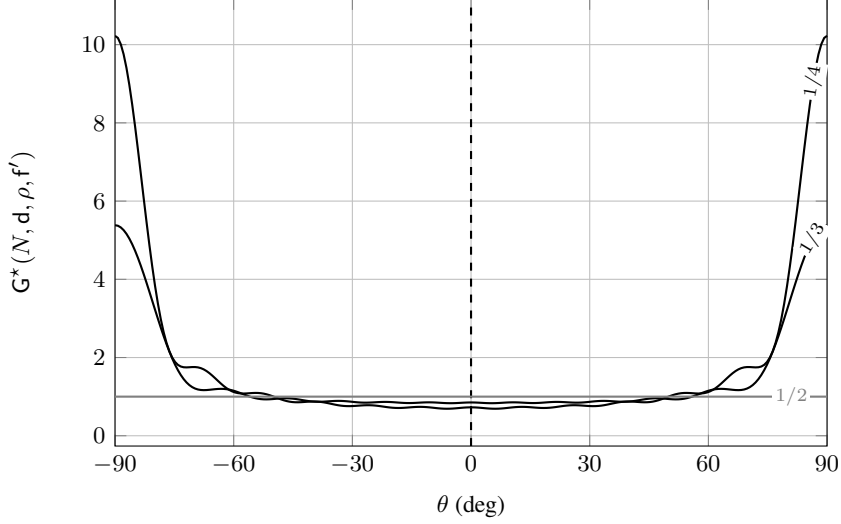


**Fig. 2:** Supergain in (36) as a function of the  $\theta(f')$  for various antenna spacings  $d$ . Array with  $N = 6$  isotropic antennas and loss factor  $\rho = 10^{-16}$ . Letting  $d < 1/2$  ignites coupling effects, which redistribute power density towards the endfire directions.

Also, multiplying each side of the eigenvalue equation in (33) by  $(\mathbf{j}^*)^H$  while using the constraint gives

$$\lambda^* = (\mathbf{j}^*)^H \mathbf{A}(f') \mathbf{j}^* = G^*(N, d, \rho, f'). \quad (35)$$

Plugging (34) into (35) and using the constraint in (33) yields [12]

$$G^*(N, d, \rho, f') = \mathbf{a}^H(f') \mathbf{C}^{-1}(d, \rho) \mathbf{a}(f') \quad (36)$$

while the  $Q$  factor, evaluated for  $\mathbf{j}^*$ , is

$$Q^*(N, d, \rho, f') = \frac{\|\mathbf{C}(d, \rho)^{-1} \mathbf{a}(f')\|^2}{\mathbf{a}(f')^H \mathbf{C}(d, \rho)^{-1} \mathbf{a}(f')}. \quad (37)$$

Averaging (36) over  $f'$  correctly yields 1 for lossless antennas, confirming that any supergain necessarily comes at the expense of reduced gain elsewhere. This is consistent with energy conservation and indicates that coupling can only redistribute power across visible directions, depending on  $d$ . This is exemplified in Fig. 2 where  $G^*(N, d, \rho, f')$  is plotted as a function of  $\theta = \sin^{-1}(f'/d)$  over the visible region, for  $N = 6$  antennas,  $\rho = 10^{-16}$ , and various  $d$ . As  $d$  falls below  $1/2$ , coupling arises, redistributing power towards the endfire directions. Although numerical results must be interpreted with care, due to the ill-conditioning of  $\mathbf{C}$  as  $d$  shrinks, they show the correct behavior for moderate  $N$  values. This ill-conditioning manifests in (33) as an expanding—encompassing more directions  $f'$ —intersection between the space spanned by the eigenvectors of  $\mathbf{C}$  corresponding to arbitrarily small eigenvalues and the nullspace of  $\mathbf{A}(f')$ , resulting in numerical instability [30].

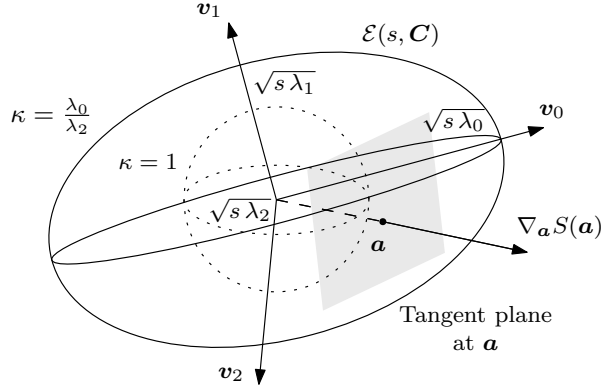


**Fig. 3:** Geometric interpretation for  $N = 3$ . The supergain factor defines an ellipsoidal surface, with each point  $\mathbf{a}$  corresponding to a physical direction via the mapping  $f \mapsto \mathbf{a}$  in (17). The ellipsoid’s eccentricity encodes the dynamic range (maximum-to-minimum elongation), while the  $Q$  factor quantifies the local rate of change near any point on the surface.

## 4.2 Geometric Interpretation

From the mapping  $f' \mapsto \mathbf{a}$  in (17), the level set defined by  $G^*(N, \mathbf{d}, \rho, \mathbf{a}) = s$  in (36) describes the surface of an  $N$ -dimensional ellipsoid, namely (see Fig. 3)

$$\mathcal{E}(s, \mathbf{C}) = \{\mathbf{a} : \|\mathbf{a}\| = 1, \mathbf{a}^H (s \mathbf{C})^{-1} \mathbf{a} = 1\}, \quad (38)$$

for  $\text{tr}(\mathbf{C}) = N(1 + \rho)$  and every admissible  $s$ , meaning  $s \in [\lambda_0^{-1}, \lambda_{N-1}^{-1}]$ . The extrema of (36) occur when  $\mathbf{a}$  aligns with either the maximum- or the minimum-eigenvalue eigenvector, respectively  $\mathbf{v}_0$  or  $\mathbf{v}_{N-1}$ , giving

$$\max_{\mathbf{a}: \|\mathbf{a}\|=1} G^*(N, \mathbf{d}, \rho, \mathbf{a}) = \frac{1}{\lambda_{N-1}(N, \mathbf{d}, \rho)} \quad \min_{\mathbf{a}: \|\mathbf{a}\|=1} G^*(N, \mathbf{d}, \rho, \mathbf{a}) = \frac{1}{\lambda_0(N, \mathbf{d}, \rho)}. \quad (39)$$

For  $\mathbf{d} = 1/2$ , it holds that  $\mathbf{C} = (1 + \rho)\mathbf{I}$  and the ellipsoid collapses into a unit-radius hypersphere. As  $\mathbf{d}$  shrinks, coupling deforms this sphere into an ellipsoid introducing an anisotropic scaling specified by  $\mathbf{C}$  (see again Fig. 3). The ratio between the squared major and minor semi-axis lengths or eccentricity of the ellipsoid equals the supergain’s dynamic range

$$\kappa(N, \mathbf{d}, \rho) = \frac{\max_{\mathbf{a}: \|\mathbf{a}\|=1} G^*(N, \mathbf{d}, \rho, \mathbf{a})}{\min_{\mathbf{a}: \|\mathbf{a}\|=1} G^*(N, \mathbf{d}, \rho, \mathbf{a})} = \frac{\lambda_0(N, \mathbf{d}, \rho)}{\lambda_{N-1}(N, \mathbf{d}, \rho)} \geq 1, \quad (40)$$

which coincides with the condition number of  $\mathbf{C}$ , with equality in the uncoupled case.

At any point  $\mathbf{a} = \mathbf{a}(f')$  on the level set, from (37),

$$Q^*(N, \mathbf{d}, \rho, \mathbf{a}) = s^{-1} \|\mathbf{C}^{-1}(\mathbf{d}, \rho) \mathbf{a}\|^2 \quad (41)$$

$$= \frac{s^{-1}}{4} \|\nabla_{\mathbf{a}} G^*(N, \mathbf{d}, \rho, \mathbf{a})\|^2 \quad (42)$$

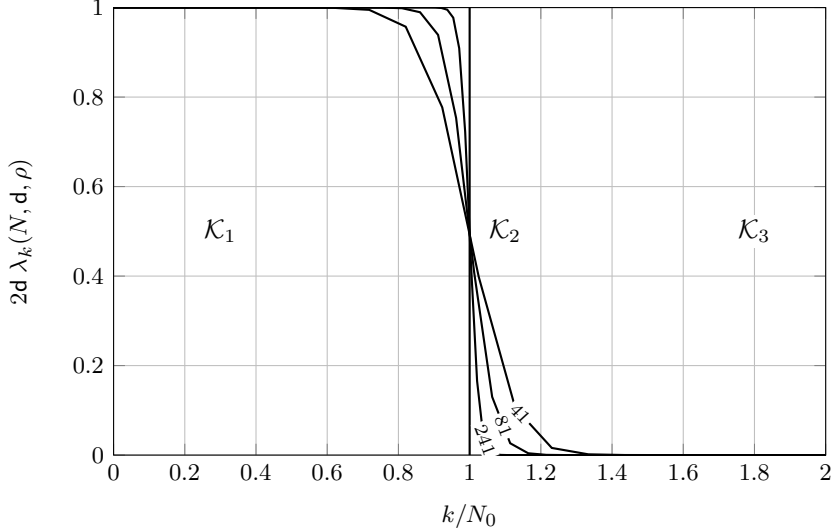


**Fig. 4:** Normalized sorted eigenvalues of the coupling matrix  $\mathbf{C}(d, \rho)$  for various  $N$  (corresponding to apertures of electrical size  $L = 5, 10, 30$ ) with  $d = 1/8$  and  $\rho = 10^{-16}$ . The eigenvalue indexes are normalized to reveal the asymptotic polarization of the curves as the aperture increase relative to the wavelength. This asymptotic behavior naturally partitions the index set into three regions:  $\mathcal{K}_1$  and  $\mathcal{K}_3$ , where the eigenvalues respectively concentrate near 1 and 0, and  $\mathcal{K}_2$ , which defines the transition region.

where  $\nabla_{\mathbf{a}} G^* = 2\mathbf{C}^{-1}\mathbf{a}$  is the gradient vector of  $G^*$  with respect to  $\mathbf{a}$ . This vector is normal to the ellipsoid's surface and its norm quantifies the rate of change of  $G^*$  at that point. Thus, the  $Q$  factor measures the sensitivity of supergain to perturbations in directionality around any  $\mathbf{a}$ .

This geometric interpretation clarifies why a high supergain is always accompanied by a high  $Q$  factor, while the converse need not hold [25, 26]. Anisotropic ellipsoids exhibit steep gradients near their elongated axes, where supergain is highest. This results in both large  $G^*$  and high  $Q^*$ . Conversely, sharp bumps in the ellipsoid's surface can also arise in regions where supergain is moderate, due to local curvature, yielding a high  $Q$  for small values of  $S$ .

### 4.3 Regimes of High Supergain

From (36), supergains much higher than unity require that the coupling matrix  $\mathbf{C}$  be poorly conditioned. Such high supergains are attained along directions specified by  $f'$  for which  $\mathbf{a}(f')$  intersects the essential nullspace of  $\mathbf{C}$ —spanned by eigenvectors associated with eigenvalues that are practically zero [13]. In these directions, the optimal current distribution (34) sustains a strong reactive field, as evidenced by  $Q^* \gg 1$  in (37). This is consistent with supergains relying on the excitation of evanescent waves associated with spatial frequencies in the invisible spectrum [31]. Such waves decay exponentially and contribute solely to reactive power, rather than to far-field radiation [13, 24].

The optimal currents are inherently unstable and highly sensitive to small perturbations in the antenna excitations or positions [8]. Antenna losses mitigate this behavior through  $\rho$  in

(27), acting as a physical regularization that elevates the small eigenvalues of  $\mathbf{C}$ , improving conditioning while limiting the achievable supergain.

As small eigenvalues indicate strong coupling, the expansion of the essential nullspace of  $\mathbf{C}$  reflects a surge in coupling. Two distinct regimes in which this occurs are next examined.

- For a given  $N$ , supergain arises as  $d$  shrinks, implying a downsize of the aperture in wavelength units [4, 5]. As  $d \rightarrow 0$ , the array collapses into a single antenna, as reflected by  $\mathbf{C}$  effectively becoming rank-1. In this limit, the array *spatially concentrates*, leading to a quadratic scaling of the endfire gain for lossless antennas [7], corresponding to a linear scaling of the endfire supergain factor, namely

$$\lim_{d \rightarrow 0} D_{\parallel}^*(N, d) = N. \quad (43)$$

Antenna losses via  $\rho$  induce a unimodal dependence of  $G_{\parallel}^*$  on  $d$ , instead of the monotonic behavior observed in the lossless case as  $d$  shrinks [11, 12]. The supergain peak now occurs at a nonzero  $d$ , which is determined by  $N$  and  $\rho$ , making such gains achievable in practice through realizable antennas. The asymptotic behavior in the spatial concentration regime is quantified in Section 7.

- A complementary mechanism to spatial concentration is *spectral concentration*. Both mechanisms drive some eigenvalues of  $\mathbf{C}$  toward zero, but they act in distinct domains. Spectral concentration yields supergain through an increase in  $N$ , for fixed  $d < 1/2$ , implying a widening aperture in wavelength units. Fig. 4 illustrates this phenomenon by plotting the ordered eigenvalues of  $\mathbf{C}$  for growing  $N$  and  $d = 1/16$ ,  $\rho = 10^{-16}$ . As the aperture widens, the eigenvalues polarize into 0 and 1, the transition between the two levels occurring at the index [32]

$$N_0 = 2dN. \quad (44)$$

This number represents the spatial degrees of freedom (DOF) of the array, up to an error of order  $\mathcal{O}(\log N)$ , which characterizes the width of the transition region. Hence, normalizing the eigenvalue indices by  $N_0$  reveals the concentration as  $N \rightarrow \infty$  by also concealing other effects—such as the impact of inherent losses—asymptotically.

The eigenvalue polarization asymptotically partitions the array into  $N_0$  uncoupled antennas and  $N - N_0 = N(1 - 2d)$  fully coupled ones. Since full coupling generates a linear endfire supergain factor, this leads to

$$\lim_{N \rightarrow \infty} \frac{D_{\parallel}^*(N, d)}{N} = \tau(d), \quad (45)$$

with the impact of  $d$  subsumed into the scaling factor  $0 < \tau(d) < 1$ . Particularly,  $\tau(d)$  approaches 0 as  $d \rightarrow 1/2$  and 1 as  $d \rightarrow 0$ , respectively. Accounting for losses via  $\rho$ , the behavior in (45) persists provided that the essential nullspace of the coupling matrix continues to grow with  $N$ . The asymptotic scaling factor  $\tau(d)$  and the loss factor  $\rho$  compatible with the spectral concentration sustaining this scaling are quantified in Section 8.

## 5 Concentration in the Discrete-Space Domain

This section recalls several results on the concentration of discrete-space sequences, enabling the subsequent quantitative analysis of supergain. The formulation transposes the classical time-domain analysis [32–37] to the spatial domain, leveraging the isomorphism between the two domains established in Section 2.1. Comprehensive derivations for the more intricate results are deferred to Appendix A.

**Definition 1** (Indexlimited and Bandlimited Sequences [37, 38]). *Let  $\mathcal{I}_N$  and  $\mathcal{B}_d$  be the subspaces of unit-norm sequences supported on the index set  $[N]$  defined in (1) and whose spectra are supported in  $[-d, d]$ , respectively. The indexlimiting operator  $I_N$  truncates a sequence  $\{x_n\}_{n \in \mathbb{Z}}$  to  $[N]$ :*

$$(I_N x)_n = \mathbb{1}_{[N]}(n)x_n = \begin{cases} x_n & n \in [N] \\ 0 & \text{otherwise} \end{cases} \quad (46)$$

while the bandlimiting operator  $B_d$  reconstructs  $x_n$  from its spectrum  $X(f)$  by retaining only components within the spatial bandwidth  $d$ ,

$$(B_d x)_n = F^{-1} \mathbb{1}_{[-d, d]}(f) F x_n = \int_{-d}^d X(f) e^{j2\pi f n} df. \quad (47)$$

Both  $I_N$  and  $B_d$  act as orthogonal projections (in the  $\mathcal{L}^2$  sense) onto  $\mathcal{I}_N$  and  $\mathcal{B}_d$ .

The asymptotic dimension of the space spanned by sequences that are simultaneously concentrated in both space and spatial frequency is formalized next.

**Definition 2** (Spatial Degrees of Freedom [32, 35, 39]). *Let  $j_n \in \mathcal{I}_N$  with its spectrum  $J(f)$  being  $\epsilon_d$ -concentrated in  $\mathcal{B}_d$ . Denote by  $N_0(N, d, \epsilon_d, \epsilon)$  the minimum number of basis functions  $U_0(N, d, f), \dots, U_{N_0-1}(N, d, f)$  with indexlimited Fourier inverse transform required to approximate—through linear combination with some expansion coefficients  $\{J_k\}$ —any spectrum  $J(f)$  over  $[-d, d]$  with  $\epsilon$ -accuracy,*

$$N_0 = 1 + \min \left\{ M \in \mathbb{N}_0 : \left\| J - \sum_{k=0}^{M-1} J_k U_k \right\|_{[-d, d]} \leq \epsilon \right\} \quad 0 \leq \epsilon_d < \epsilon < 1. \quad (48)$$

Asymptotically,

$$\lim_{N \rightarrow \infty} \frac{N_0(N, d, \epsilon_d, \epsilon)}{N} = 2d, \quad (49)$$

with the lower-order dependence on  $\epsilon_d$  and  $\epsilon$  vanishing. For  $d = 1/2$ ,  $N_0 = N$ .

Since the norm in (48) represents the residual energy outside the subspace spanned by the basis functions, the optimal subspace consists of the indexlimited sequences whose spectra  $U_k(N, d, f)$  are most concentrated within  $[-d, d]$  [37, Ch. 2]. These are obtained as solutions of the following eigenvalue problem.

**Lemma 1** (Maximally Concentrated Spectra [32, 37]). *Let  $D_N(\mathbf{f})$  be the Dirichlet kernel in (21). The ordered eigenfunctions  $U_0(N, \mathbf{d}, \mathbf{f}), \dots, U_{M-1}(N, \mathbf{d}, \mathbf{f})$  solving [32, Eq. 10]*

$$\int_{-\mathbf{d}}^{\mathbf{d}} D_N(\mathbf{f} - \mathbf{g}) U_k(N, \mathbf{d}, \mathbf{g}) d\mathbf{g} = \mu_k(N, \mathbf{d}) U_k(N, \mathbf{d}, \mathbf{f}) \quad |\mathbf{f}| \leq \mathbf{d}, \quad (50)$$

*span an optimal  $M$ -dimensional subspace of  $\mathcal{S}_N$  for any  $M \leq N$ . The kernel's real symmetry and positive-definiteness ensure that the ordered eigenvalues  $1 > \mu_0 > \dots > \mu_{N-1} > 0$  are real and distinct, and that the eigenfunctions are unique and orthogonal over  $[-\mathbf{d}, \mathbf{d}]$ .*

Solving the concentration problem in (50) is made possible by establishing a correspondence with a well-known ordinary differential equation.

**Lemma 2** (Discrete prolate spheroidal wave functions [32]). *The eigenfunctions  $U_0(N, \mathbf{d}, \mathbf{f}), \dots, U_{N-1}(N, \mathbf{d}, \mathbf{f})$  are also solution to the Sturm-Liouville eigenvalue problem*

$$M U = \theta U, \quad (51)$$

*induced by the second-order homogeneous differential operator*

$$M = \frac{1}{(2\pi)^2} \frac{d}{d\mathbf{f}} \left\{ (\cos(2\pi\mathbf{f}) - A) \frac{d}{d\mathbf{f}} \right\} + \frac{N^2 - 1}{4} \cos(2\pi\mathbf{f}), \quad (52)$$

*where*

$$A = \cos(2\pi\mathbf{d}). \quad (53)$$

*These eigenfunctions are associated with a discrete set of real positive values of  $\theta$ , the eigenvalues of  $M$ , namely  $\theta_0(N, \mathbf{d}) > \dots > \theta_{N-1}(N, \mathbf{d}) > 0$ .*

The correspondence between the concentration problem in (50) and ordinary differential equation in (52) reveals detailed information about the structure of the  $U_k$ 's.

**Remark 1** (Symmetry and Zeros [32]). *The eigenfunctions  $U_0(N, \mathbf{d}, \mathbf{f}), \dots, U_{N-1}(N, \mathbf{d}, \mathbf{f})$  form a complete set in  $\mathcal{L}^2[-\frac{1}{2}, \frac{1}{2}]$ . Each  $U_k$  is symmetric for even  $k$  and antisymmetric for odd  $k$ , with period 1 when  $N$  is odd. It has  $N - 1$  simple zeros in  $[-\frac{1}{2}, \frac{1}{2}]$ , of which  $k$  are within the open interval  $(-\mathbf{d}, \mathbf{d})$ .*

**Corollary 1** (Duality [32]). *The ordered eigenvalues  $\mu_0, \dots, \mu_{N-1}$  in (50) are also the real solution to the Hermitian counterpart operator of (50),*

$$\mathbf{\Omega}(\mathbf{d}) \mathbf{v}_k(N, \mathbf{d}) = \mu_k(N, \mathbf{d}) \mathbf{v}_k(N, \mathbf{d}) \quad k = 0, \dots, N - 1, \quad (54)$$

*where  $\mathbf{\Omega} \in \mathbb{R}^{N \times N}$  is the real, symmetric, and positive-definite prolate matrix with entries*

$$[\mathbf{\Omega}(\mathbf{d})]_{n,m} = \frac{\sin(2\pi\mathbf{d}(n - m))}{\pi(n - m)} \quad n, m \in [N]. \quad (55)$$

This matrix admits a unique set of real orthonormal eigenvectors  $\mathbf{v}_0(N, \mathbf{d}), \dots, \mathbf{v}_{N-1}(N, \mathbf{d})$ , each equals the discrete prolate spheroidal sequence  $v_n^{(k)}(N, \mathbf{d})$  indexlimited to  $[N]$ .

**Lemma 3** (Fourier relationship [32]). *The discrete prolate spheroidal sequences and discrete prolate spheroidal wave functions are related by*

$$U_k(N, \mathbf{d}, \mathbf{f}) = \epsilon_k \sqrt{N} \mathbf{a}(\mathbf{f})^H \mathbf{v}_k(N, \mathbf{d}) \quad |\mathbf{f}| \leq \frac{1}{2}, \quad (56)$$

where  $\mathbf{a}(\mathbf{f})$  is defined in (17) and  $\epsilon_k$  is 1 or  $j$  depending on whether  $k$  is even or odd. Conversely,

$$\mathbf{v}_k(N, \mathbf{d}) = \frac{\sqrt{N}}{\epsilon_k} \int_{-1/2}^{1/2} U_k(N, \mathbf{d}, \mathbf{f}) \mathbf{a}(\mathbf{f}) d\mathbf{f}, \quad (57)$$

confirming that the sequences, whose spectra are  $U_k(N, \mathbf{d}, \mathbf{f})$ , belong to  $\mathcal{I}_N$ . Also,

$$U_k(N, \mathbf{d}, \mathbf{f}) = \epsilon_k \mu_k(N, \mathbf{d}) \sum_{n \in \mathbb{Z}} v_n^{(k)}(N, \mathbf{d}) e^{-j2\pi \mathbf{f}n} \quad |\mathbf{f}| \leq \mathbf{d}, \quad (58)$$

consistent with the spectrum of  $v_n^{(k)}(N, \mathbf{d})$  being in  $\mathcal{B}_d$ . Also,  $\epsilon_k$  ensures real-valued sequences for all  $k$ , consistent with the symmetry of  $U_k(N, \mathbf{d}, \mathbf{f})$ .

**Corollary 2** (Double Orthogonality [32, 36]). *Under the normalization conditions  $\|U_k\| = 1$  and  $\|\mathbf{v}_k\| = 1$ , the discrete prolate spheroidal wave functions and corresponding sequences satisfy, for  $k, \ell = 0, \dots, N-1$ ,*

$$\int_{-d}^d U_k(N, \mathbf{d}, \mathbf{f}) U_\ell(N, \mathbf{d}, \mathbf{f}) d\mathbf{f} = \mu_k(N, \mathbf{d}) \int_{-1/2}^{1/2} U_k(N, \mathbf{d}, \mathbf{f}) U_\ell(N, \mathbf{d}, \mathbf{f}) d\mathbf{f} = \mu_k(N, \mathbf{d}) \delta_{k\ell} \quad (59)$$

$$\mathbf{v}_k(N, \mathbf{d})^T \mathbf{v}_\ell(N, \mathbf{d}) = \mu_k(N, \mathbf{d}) \sum_{n \in \mathbb{Z}} v_n^{(k)}(N, \mathbf{d}) v_n^{(\ell)}(N, \mathbf{d}) = \delta_{k\ell}. \quad (60)$$

From Corollary 2, each eigenfunction  $U_k(N, \mathbf{d}, \mathbf{f})$  contains a fraction  $0 < \mu_k < 1$  of its energy within  $[-d, d]$  [37, Sec. 2.5]. The principal eigenfunction  $U_0$  achieves the highest concentration  $\mu_0$ , followed by  $U_1, U_2, \dots$  with progressively lower concentration  $\mu_1, \mu_2, \dots$

**Remark 2** (Orthogonal Basis [32]). *The sequences  $v_n^{(0)}, \dots, v_n^{(N-1)}$  form an orthogonal basis for  $\mathcal{B}_d$ . Similarly, the truncated sequences  $\mathbf{v}_0(N, \mathbf{d}), \dots, \mathbf{v}_{N-1}(N, \mathbf{d})$  form an orthonormal basis for  $\mathcal{I}_N$ . Consequently, any  $j_n \in \mathcal{B}_d$  (respectively, any  $\mathbf{j} \in \mathcal{I}_N$ ) admits a unique expansion in terms of  $\{v_n^{(k)}(N, \mathbf{d})\}$  (respectively,  $\{\mathbf{v}_k(N, \mathbf{d})\}$ ).*

## 6 Concentration of Uniform Linear Arrays

### 6.1 Spectral Representation

From Remark 2, any indexlimited current  $\mathbf{j} \in \mathcal{J}_N$  admits the orthogonal representation

$$\mathbf{j}(N, \mathbf{d}) = \sum_{k=0}^{N-1} \epsilon_k J_k(N, \mathbf{d}) \mathbf{v}_k(N, \mathbf{d}). \quad (61)$$

A discrete-space Fourier transform of both sides as per (2) gives the spectral representation

$$J(\mathbf{f}) = \sum_{k=0}^{N-1} J_k(N, \mathbf{d}) U_k(N, \mathbf{d}, \mathbf{f}) \quad |\mathbf{f}| \leq \frac{1}{2}, \quad (62)$$

where  $U_k(N, \mathbf{d}, \mathbf{f})$  appears because of (56). By the double orthogonality of the  $U_k$ 's (see (59) in Corollary 2), the coefficients can be found to be

$$J_k(N, \mathbf{d}) = \int_{-1/2}^{1/2} J(\mathbf{f}) U_k(N, \mathbf{d}, \mathbf{f}) d\mathbf{f} = \frac{1}{\mu_k(N, \mathbf{d})} \int_{-\mathbf{d}}^{\mathbf{d}} J(\mathbf{f}) U_k(N, \mathbf{d}, \mathbf{f}) d\mathbf{f}, \quad (63)$$

satisfying

$$\sum_{k=0}^{N-1} |J_k(N, \mathbf{d})|^2 = 1 \quad (64)$$

by virtue of (10) and Parseval's theorem. Building on the link between spatial coupling and spectral concentration, Appendix B derives the supergain factor at any spatial frequency  $\mathbf{f}'$  as

$$\mathbf{G}^*(N, \mathbf{d}, \rho, \mathbf{f}') = \frac{1}{N} \sum_{k=0}^{N-1} \frac{|U_k(N, \mathbf{d}, \mathbf{f}')|^2}{\lambda_k(N, \mathbf{d}, \rho)}, \quad (65)$$

where the sum reflects the orthogonality of  $\{U_k(N, \mathbf{d}, \mathbf{f})\}$ . The corresponding  $Q$  factor is

$$Q^*(N, \mathbf{d}, \rho) = \frac{1}{C(N, \mathbf{d}, \rho, \mathbf{f}')} \left( \sum_{k=0}^{N-1} \frac{|U_k(N, \mathbf{d}, \mathbf{f}')|^2}{\lambda_k(N, \mathbf{d}, \rho)} \right)^{-1}, \quad (66)$$

where

$$\frac{1}{C(N, \mathbf{d}, \rho, \mathbf{f}')} = \sum_{k=0}^{N-1} \frac{|U_k(N, \mathbf{d}, \mathbf{f}')|^2}{\lambda_k^2(N, \mathbf{d}, \rho)} \quad (67)$$

to enforce (64). Such supergain and  $Q$  factors are attained by the optimal coefficients

$$J_k^*(N, \mathbf{d}, \rho, \mathbf{f}') = \frac{\sqrt{C(N, \mathbf{d}, \rho, \mathbf{f}')} U_k(N, \mathbf{d}, \mathbf{f}')}{\lambda_k(N, \mathbf{d}, \rho)}, \quad (68)$$

which yield the maximum-gain spectrum

$$J^*(\mathbf{d}, \rho, \mathbf{f}', \mathbf{f}) = \sqrt{C(N, \mathbf{d}, \rho, \mathbf{f}')} \sum_{k=0}^{N-1} \frac{U_k(N, \mathbf{d}, \mathbf{f}')}{\lambda_k(N, \mathbf{d}, \rho)} U_k(N, \mathbf{d}, \mathbf{f}). \quad (69)$$

Inverting (69) as per (3) while using (57) gives the corresponding current vector

$$\mathbf{j}^*(\mathbf{d}, \rho, \mathbf{f}') = \sqrt{C(N, \mathbf{d}, \rho, \mathbf{f}')} \sum_{k=0}^{N-1} \frac{\epsilon_k U_k(N, \mathbf{d}, \mathbf{f}')}{\lambda_k(N, \mathbf{d}, \rho)} \mathbf{v}_k(N, \mathbf{d}). \quad (70)$$

## 6.2 Prolate Matrix and Isotropic Coupling Matrix

To align with the spatial-domain formulation of Section 3, the lossless coupling matrix  $C(\mathbf{d})$  in (26) can be related to the  $N$ -dimensional prolate matrix  $\Omega(\mathbf{d})$  in (55) via

$$C(\mathbf{d}) = (2\mathbf{d})^{-1} \Omega(\mathbf{d}). \quad (71)$$

Note that the coupling matrix is well-defined even for  $\mathbf{d} = 0$ . The two matrices share the same eigenvectors,  $\mathbf{v}_k(N, \mathbf{d})$ , while their eigenvalues differ by a constant factor, specifically

$$\lambda_k(N, \mathbf{d}) = (2\mathbf{d})^{-1} \mu_k(N, \mathbf{d}) \quad (72)$$

$$= \frac{1}{2\mathbf{d}} \int_{-\mathbf{d}}^{\mathbf{d}} |U_k(N, \mathbf{d}, \mathbf{f})|^2 d\mathbf{f} = \frac{1}{2\mathbf{d}} \|U_k\|_{[-\mathbf{d}, \mathbf{d}]}. \quad (73)$$

From (73), each eigenvalue of the coupling matrix represents the *average* spectral concentration of the unit-norm spectrum  $U_k(N, \mathbf{d}, \mathbf{f})$  over  $[-\mathbf{d}, \mathbf{d}]$ .

Prolate matrices are classically encountered in the study of statistical correlation, where they capture the covariance in limited domains. Their emergence in the analysis of coupling is not coincidental, rather it reflects a deep isomorphism between correlation and coupling [2].

For  $\mathbf{d} = \frac{1}{2}$ , the prolate and coupling matrices reduce to the identity matrix for lossless antennas. Since there is then only one eigenvalue equal to unity with multiplicity  $N$ , the orthonormal basis  $\{\mathbf{v}_k(N, \frac{1}{2})\}$  is not unique and can be chosen arbitrarily. Without symmetry constraints, selecting the canonical basis of  $\mathbb{R}^N$ ,  $\mathbf{v}_k(N, \frac{1}{2}) = \mathbf{e}_k$ , yields the discrete Fourier transform  $U_k(N, \frac{1}{2}, \mathbf{f}) = e^{-j2\pi\mathbf{f}(k-(N-1)/2)}$  via (56) (omitting the normalization factor  $\epsilon_k$  enforcing such symmetries). Plugging this expression into (67) with  $\rho = 0$  reveals  $C = N^{-1}$ . And, applying a change of variable and using (21), (69) reduces to the Dirichlet kernel in (20),

$$J^*(\frac{1}{2}, 0, \mathbf{f}', \mathbf{f}) = \frac{1}{\sqrt{N}} \sum_{k=0}^{N-1} e^{-j2\pi(\mathbf{f}-\mathbf{f}')\left(k-\frac{N-1}{2}\right)} = \frac{D_N(\mathbf{f}-\mathbf{f}')}{\sqrt{N}}. \quad (74)$$

For  $\mathbf{d} < 1/2$ , the spectrum of (34) follows by substituting (56) into (69), noticing that  $\mathbf{v}_k(N, \mathbf{d})$  are the eigenvectors of the coupling matrix and  $|\epsilon_k| = 1$  (since  $\epsilon_k$  equals 1 or  $j$ ).

## 7 Spatial Concentration

For vanishing  $d$ , the  $U_k$ 's converge, up to a scalar factor, to Legendre polynomials [32]. This asymptotic correspondence, detailed in Appendix C, characterizes the eigenstructure of (51) with eigenvalues satisfying

$$\theta_k(N, d) = \frac{N^2 - 1}{4} - \frac{k(k+1)}{2} + \mathcal{O}(d) \quad (75)$$

and corresponding eigenfunctions satisfying

$$U_k(N, d, f) = P_k\left(\frac{f}{d}\right) + \mathcal{O}(d^2), \quad (76)$$

where  $P_k$  is the Legendre polynomial of degree  $k$ , for  $k = 0, \dots, N-1$ . These polynomials obey the orthogonality relation [40, Eq. 22.2.1]

$$\int_{-1}^1 P_k(y)P_\ell(y) dy = \frac{2}{2k+1} \delta_{\ell k}, \quad (77)$$

forming an orthogonal basis on  $\mathcal{L}^2[-1, 1]$  as a function of  $y = f/d$ .

Exploiting the Legendre eigenstructure, and that the associated  $\lambda_k$ 's are the corresponding average spectral concentrations over  $[-d, d]$  asymptotically, Appendix D analyzes the supergain factor in (65) along specific directions as  $d$  vanishes for fixed  $N$  and  $\rho$ . Two distinct regimes emerge, according to  $\rho$  relative to  $N$ .

- For  $\rho N \ll 1$ ,

$$G_{\parallel}^*(N, d, \rho) = N - \frac{\rho}{3}(N-1)(4N+1) + \mathcal{O}(\rho N), \quad (78)$$

which subsumes the classical supergain result in (43) whenever  $\rho = 0$ ; the second term in (78) represents the correction due to antenna losses. Since any supergain enhancement must be offset by a reduction elsewhere, the broadside direction reflects this complementary behavior, yielding, for vanishing  $d$  and large  $N$ ,  $D_{\perp}^*(N, d) = 2/\pi + \mathcal{O}(\ln(N)/N)$ .

- When antenna losses dominate instead,  $\rho N \gg 1$ , the supergain factor is curtailed and saturates as  $N$  increases, giving

$$G_{\parallel}^*(N, d, \rho) = \frac{1}{\rho} - \frac{1-\rho}{2\rho^2} \frac{\ln N}{N} + \mathcal{O}\left(\frac{1}{N}\right). \quad (79)$$

Unraveling the normalization in (29), the maximum endfire gain now grows only linearly with  $N$ ; its slope is  $\rho^{-1}$ , quantifying how more efficient antennas sustain a steeper growth than their less efficient counterparts.

## 8 Spectral Concentration

### 8.1 Asymptotic Behavior

For widening apertures ( $N \rightarrow \infty$ ) with fixed antenna spacing, the eigenstructure of the solution to (51) depends on the spatial frequency  $f$  within  $[-d, d]$  and the index  $k$  [32, Sec. 4.2]. For large  $N$ , with the substitution

$$G(f) = U(f) \sqrt{\cos(2\pi f) - A} \quad (80)$$

and the eigenvalue expansion

$$\theta(B) = \frac{1}{4} B N^2 + \frac{1}{4} C N + \mathcal{O}(1), \quad (81)$$

where  $A$  is defined in (53),  $B$  satisfies  $-1 < A \leq B \leq 1$ , and  $C$  is a free parameter (specified later) that depends on  $B$ , the Sturm-Liouville eigenvalue problem in (51) is cast in the Schrödinger form [32, Eq. 135]

$$\frac{d^2 G(f)}{df^2} = N^2 P(B, f) G(f). \quad (82)$$

For the problem at hand,

$$P(B, f) = \left( \frac{\pi}{\cos(2\pi f) - A} \right)^2 (\cos(2\pi f) - y_0)(y_1 - \cos(2\pi f)), \quad (83)$$

which captures the dependence of (82) on  $\theta$ , subsumed into the roots  $y_0 = B + \mathcal{O}(N^{-1})$  and  $y_1 = A + \mathcal{O}(N^{-1})$ . (The inequality  $A > -1$  applied to (53) implies  $d < 1/2$  and ensures that (83) is well behaved.)

The WKB method constructs solutions to (82) for large  $N$  [41, Sec. 10], yielding

$$G(B, f) = \exp\left(-N \int_f \sqrt{P(B, g)} dg + \mathcal{O}(1)\right) \quad N \rightarrow \infty. \quad (84)$$

The sign of  $P(B, f)$  reveals the qualitative behavior of  $G(B, f)$ , and in turn of  $U(B, f)$ : both functions oscillate for  $P \leq 0$  while they are evanescent (i.e., exponentially decaying in  $f$ ) for  $P > 0$ . Specializing it to the problem at hand via (83), we have that, asymptotically in  $N$ ,

$$U(B, f) \sim \begin{cases} \text{oscillatory in } f & f \in (0, \arccos(B)/2\pi) \cup (d, \frac{1}{2}) \\ \text{evanescent in } f & f \in (\arccos(B)/2\pi, d). \end{cases} \quad (85)$$

From Lemma 2, the Sturm-Liouville eigenvalue problem has a finite number of nontrivial solutions; these are the eigenfunctions  $G_k(f) = G(B_k, f)$ , as well as  $U_k(f) = U(B_k, f)$  via

(80), and corresponding eigenvalues  $\theta_k = \theta(B_k)$ , given by

$$\theta_k = \frac{1}{4}B_k N^2 + \frac{1}{4}C_k N + \mathcal{O}(1) \quad (86)$$

with parameters  $B_k$  and  $C_k$  inheriting a dependence on the index  $k$  through the constraint [41, Sec. 10.5]

$$B_k = \left\{ A < x < 1 : N \int_0^{\arccos(x)/2\pi} \sqrt{-P(x, f)} df = \left(k + \frac{1}{2}\right) \pi + \mathcal{O}\left(\frac{1}{N}\right) \right\}. \quad (87)$$

For the problem at hand, replacing  $P(f)$  by (83) and applying the substitution  $t = \cos(2\pi f)$ ,

$$B_k = \left\{ A < x < 1 : \int_x^1 \sqrt{\frac{t-x}{(t-A)(1-t^2)}} dt \sim \frac{k\pi}{N} \right\}, \quad (88)$$

where only the leading-order term in the right-hand side of (87) was retained.

In light of (85), the position of  $B_k$  relative to the fixed endpoints  $A$  and 1 determines the spectral behavior of the  $U_k$ 's by partitioning the index set  $\{0, \dots, N-1\}$  into three subsets,  $\mathcal{K}_1, \mathcal{K}_2, \mathcal{K}_3$ . This partition mirrors the distinct asymptotic behaviors of the eigenvalues  $\mu_k$  in Fig. 4, each representing the average concentration of the associated  $U_k$  within the visible region as per (73). The dependence of  $B_k$  and  $C_k$  on  $k$  within each  $\mathcal{K}_i$  is mapped to an asymptotic parameter  $x_i$ , such that each subset is characterized by a common behavior defined by continuous variables  $B$  and  $C$ .

- $A < B < 1$  or  $\mathcal{K}_1 = \{k = \lfloor N_0(1-x_1) \rfloor, 0 < x_1 < 1\}$   
Within the visible region, the  $U_k$ 's exhibit  $k = \mathcal{O}(N)$  oscillations, consistently with Remark 1; this corresponds to a *low-pass* behavior.
- $A = B$  or  $\mathcal{K}_2 = \{k = \lfloor N_0 + \frac{x_2}{\pi} \log N \rfloor, -\frac{\pi N_0}{\log(N)} < x_2 < \frac{\pi}{\log(N)}(N - N_0)\}$   
The roots collapse at  $f = d$ , whereby oscillations extend across the entire visible region, corresponding to an *all-pass* behavior.
- $-A < B$  or  $\mathcal{K}_3 = \{k = \lfloor N_0(1+x_3) \rfloor, 0 < x_3 < \frac{1}{2d} - 1\}$   
By means of the spatial-frequency symmetry in Remark 1, this case reduces to  $\mathcal{K}_2$  with transformed variables  $f \rightarrow \frac{1}{2} - f$ , implying  $A \rightarrow -A$  and  $k \rightarrow N - k - 1$ . The visible region becomes  $d \leq f \leq \frac{1}{2}$ , revealing an intrinsic *high-pass* behavior.

Following the framework in [32], the asymptotic characterization of the  $U_k$ 's in the end-fire direction, and of their associated eigenvalues via the  $\mu_k$ 's, is formalized in Appendix E. (The characterization of the broadside behavior merely entails setting  $f = 0$  in lieu of  $|f| = d$ .) These components define the asymptotic behavior of the supergain factor in (65) through three distinct contributions from the subsets  $\mathcal{K}_1, \mathcal{K}_2$ , and  $\mathcal{K}_3$ . In  $\mathcal{K}_1$ , the exponential decay of the eigenfunctions at endfire, paired with eigenvalues near unity (see Fig. 4), renders its contribution negligible for large  $N$ , of order  $\mathcal{O}(e^{-LN})$  for  $L > 0$ . Consequently, the supergain factor is dominated by contributions from  $\mathcal{K}_2$  and  $\mathcal{K}_3$ , which yield constant or linear scaling,  $\mathcal{O}(1)$  and  $\mathcal{O}(N)$ , depending on antenna losses via  $\rho$  relative to  $N$  and  $d$ . A *supergain regime* emerges when the eigenvalues remain larger than  $\rho$ , allowing the  $\mathcal{K}_3$  contributions to

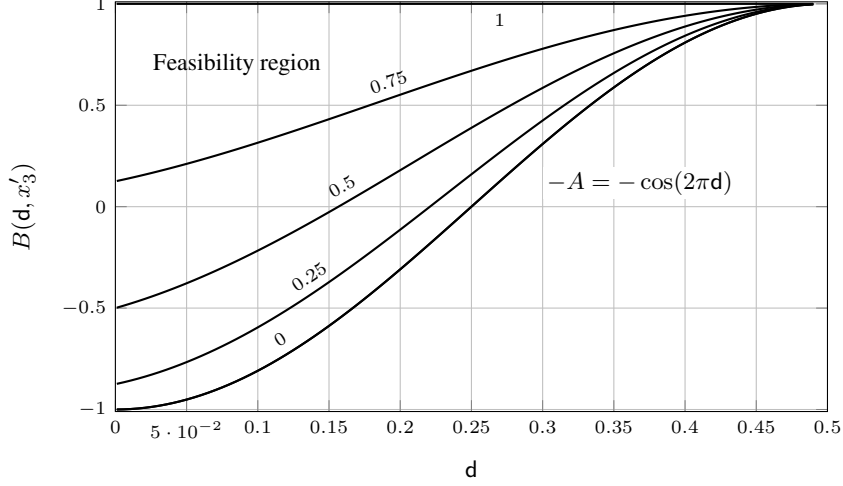


**Fig. 5:**  $B(d, x'_3)$  from (92) versus  $d$  for various  $x'_3 \in (0, 1)$ . The mapping  $x'_3 \rightarrow B$  is invertible. The curves show that  $B \rightarrow 1$  as  $x'_3 \rightarrow 1$  and  $B \rightarrow -A$  as  $x'_3 \rightarrow 0$ .

sustain a linear growth with  $N$ . Conversely, a *loss-dominated regime* occurs when  $\rho$  eclipses the smallest eigenvalues in  $\mathcal{K}_3$ , masking their contributions and causing the saturation of the supergain factor with increasing  $N$ .

Since subsets  $\mathcal{K}_2$  and  $\mathcal{K}_3$  are inherently non-disjoint, their combinations provide non-achievable bounds on the supergain: a lower bound is derived from  $\mathcal{K}_3$  alone, while an upper bound sums both subsets. As established in Appendix F, in the lossless case ( $\rho = 0$ ), these bounds are asymptotically tight because the sublinear contribution from  $\mathcal{K}_2$  vanishes (relative to that of  $\mathcal{K}_3$ ) as  $N \rightarrow \infty$ . In this limit, the sum contribution from each subset  $\mathcal{K}_i$  converges to a Riemann integral over the continuous variable  $x_i$ .

## 8.2 Operating Regimes

Let us introduce the auxiliary variable  $x'_3$ , defined asymptotically by

$$x'_3 \sim \left( \frac{1}{2d} - 1 \right)^{-1} x_3, \quad (89)$$

satisfying  $x'_3 \in (0, 1)$  for any  $0 \leq d < 1/2$ . The asymptotic behavior within  $\mathcal{K}_3$  is governed by the integrals

$$L'_i(d, x'_3) = \int_0^{\pi/2} \ell'_i(d, x'_3, \phi) d\phi \quad (90)$$

associated with the positive kernels (see Appendix E)

$$\ell'_i(\mathbf{d}, x'_3, \phi) = \begin{cases} \frac{2(1 - B(\mathbf{d}, x'_3)) \cos^2 \phi}{|[1 + A - (1 - B(\mathbf{d}, x'_3)) \sin^2 \phi] [2 - (1 - B(\mathbf{d}, x'_3)) \sin^2 \phi]|^{1/2}} & i = 1 \\ \frac{2}{|[1 + A - (1 - B(\mathbf{d}, x'_3)) \sin^2 \phi] [2 - (1 - B(\mathbf{d}, x'_3)) \sin^2 \phi]|^{1/2}} & i = 2 \\ \frac{2(A + B(\mathbf{d}, x'_3)) \sin^2 \phi}{|1 - [(A + B(\mathbf{d}, x'_3)) \sin^2 \phi - B(\mathbf{d}, x'_3)]^2|^{1/2}} & i = 3 \\ 2 \left| 1 - [(A + B(\mathbf{d}, x'_3)) \sin^2 \phi - B(\mathbf{d}, x'_3)]^2 \right|^{-1/2} & i = 4. \end{cases} \quad (91)$$

In these expressions,  $A = \cos(2\pi\mathbf{d})$  as defined in (53) and the auxiliary parameter  $B(\mathbf{d}, x'_3) \in (-A, 1)$  is implicitly defined by the asymptotic constraint

$$\int_0^{\pi/2} \frac{2(1 - B) \cos^2 \phi \, d\phi}{|[1 + A - (1 - B) \sin^2 \phi] [2 - (1 - B) \sin^2 \phi]|^{1/2}} \sim \pi(1 - 2\mathbf{d})(1 - x'_3). \quad (92)$$

The above constraint defines an invertible mapping  $x'_3 \rightarrow B$  as illustrated in Fig. 5. In turn, define

$$C(\mathbf{d}, x'_3) = \frac{4}{L'_2(\mathbf{d}, x'_3)} \left[ \frac{N}{2} L'_1(\mathbf{d}, x'_3) + \left( 2 + (-1)^{\lfloor (1-2\mathbf{d})N(1-x'_3) \rfloor} \right) \frac{\pi}{4} \right]_{\text{rem } 2\pi}, \quad (93)$$

where the integrals  $L'_1$  and  $L'_2$  are defined in (90). The parameter  $C$  satisfies  $0 \leq C \leq 8\pi/L'_2$  as per the modulo operation.

With the asymptotic foundations established, the endfire supergain is asymptotically confined as  $N \rightarrow \infty$  within respective bounds derived in Appendix G, namely

$$\underline{\mathcal{G}}_{\parallel}^*(N, \mathbf{d}, \rho) < \mathcal{G}_{\parallel}^*(N, \mathbf{d}, \rho) < \overline{\mathcal{G}}_{\parallel}^*(N, \mathbf{d}, \rho) + \Delta_{\parallel}(\mathbf{d}, \rho) \quad (94)$$

where the lower bound captures the linear scaling of the supergain factor via

$$\underline{\mathcal{G}}_{\parallel}^*(N, \mathbf{d}, \rho) \sim N \int_0^1 \frac{2\pi\mathbf{d}}{L'_2(\mathbf{d}, x'_3) \text{sinc}(2\mathbf{d})} \left( 1 + 2\mathbf{d}\rho e^{C(\mathbf{d}, x'_3)L'_4(\mathbf{d}, x'_3)/2} e^{L'_3(\mathbf{d}, x'_3)N} \right)^{-1} dx'_3, \quad (95)$$

while the gap represents the  $\mathcal{O}(1)$  contribution,

$$\Delta_{\parallel}(\mathbf{d}, \rho) \sim 12\mathbf{d} \ln \left( 1 + \frac{1}{2\mathbf{d}\rho} \right). \quad (96)$$

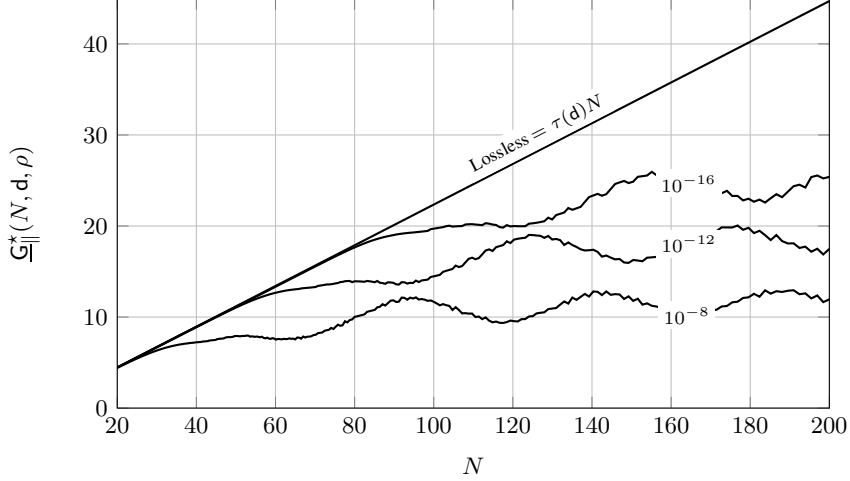


**Fig. 6:** Lower bound in (95) as a function of  $N$  for  $d = 0.45$  and various  $\rho$ . The curves are benchmarked against the lossless limit  $\tau(d)N$ . As  $N$  increases (with fixed  $\rho$  and  $d$ ), coupling gains saturate the linear scaling behavior, consistent with (97).

When the term containing  $\rho$  in (95) is far below unity, the ULA operates in the supergain regime. This requires  $\rho$  to decrease at least exponentially with growing  $N$  for fixed nonzero  $d$ ,

$$\rho = \mathcal{O}\left(e^{-L'_3 N}\right) \quad N \rightarrow \infty, \quad (97)$$

for any positive constant  $L'_3$  (The impact of such constants on the supergain factor is implicitly characterized in the numerical results.) In the regime specified by (97), the linear growth of  $\underline{G}_{\parallel}^*(N, d, \rho)$  dominates the asymptotic behavior for large  $N$  and the bounds become asymptotically tight in the sense of  $\lim_{N \rightarrow \infty} \Delta_{\parallel}(d, \rho)/N = 0$ . For  $\rho = 0$ , the scaling factor is

$$\tau(d) = \frac{2\pi d}{\text{sinc}(2d)} \int_0^1 \frac{1}{L'_2(d, x'_3)} dx'_3, \quad (98)$$

which quantifies the asymptotic linear growth with  $N$  predicted in (45). Note that the gap  $\Delta_{\parallel}(d, \rho)$  diverges as  $\rho \rightarrow 0$  resulting in an unbounded superdirectivity; see Appendix F. However, this divergence is physically inconsequential; this term is driven by contributions from the subset  $\mathcal{K}_2$  that are progressively far from the transition index  $N_0$  as  $N$  increases, rendering such components incompatible with the lossless limit  $\rho \rightarrow 0$ . The inherent physical constraints and finite apertures further regularize this behavior. Consequently, the supergain factor is expected to be dominated by the linear scaling captured by the lower bound in (95).

The lower bound in (95) is plotted in Fig. 6 against  $N$  for  $d = 0.45$  and various  $\rho$ , alongside the lossless limit  $\tau(d)N$  with slope factor  $\tau(d)$  defined in (98). (The fluctuations in the numerical results arise from the phase discontinuity in (93).) The figure shows that even the slightest deviation from a half-wavelength spacing can produce linear supergains, provided

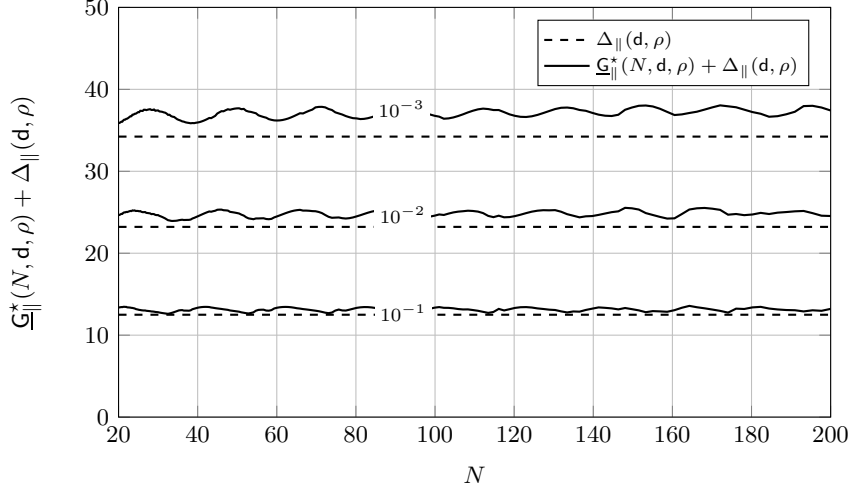


**Fig. 7:** Upper bound in (94) as a function of  $N$  for  $d = 0.45$  and various  $\rho$ . As  $\rho$  increases (with fixed  $N$  and  $d$ ), the supergain factor hinges progressively less on  $N$  and more on  $d$  and  $\rho$  through the gap term  $\Delta_{\parallel}(d, \rho)$  in (96).

that losses decay according to (97), thereby sustaining this asymptotic scaling. The failure to do so eclipses the linear behavior in favor of a constant scaling, as illustrated in Fig. 7. In this case, the ULA enters the loss-dominated regime, where the supergain factor ceases to grow with  $N$  and saturates approximately as  $\Delta_{\parallel}(d, \rho)$  in (96). This behavior emerges as losses intensify, causing the contributions to progressively concentrate within the subset  $\mathcal{K}_2$  and capturing the transition around  $N_0$  (see Fig. 4).

The supergain behavior with decreasing  $d$  for a fixed large  $N$  is illustrated in Fig. 8. Expectedly, the lossless scaling factor  $\tau(d)$  in (98) vanishes as  $d \rightarrow 1/2$ , as half-wavelength spacing suppresses mutual coupling among isotropic antennas. In contrast,  $\tau(d) \rightarrow 1$  as  $d \rightarrow 0$  (see Appendix G and the discussion preceding (45)).

When losses are included via the lower bound  $\underline{G}_{\parallel}^*(N, d, \rho)/N$ , however, the behavior deviates significantly from the lossless limit. For fixed  $\rho$ , reducing  $d$  from  $1/2$  initially increases the slope monotonically, confirming the constructive effect of coupling. Yet this trend only persists down to a critical space, beyond which the curves become unimodal, and the supergain factor rapidly deteriorates as  $d$  decreases further, consistent with [12]. As shown in Appendix H, maintaining supergain at fixed  $N$  and vanishing  $d$  requires  $\rho$  to decrease at least polynomially with  $d$ , i.e.,

$$\rho = \mathcal{O}(d^{\gamma N}) \quad d \rightarrow 0, \quad (99)$$

for any positive constant  $\gamma$ . Since  $\rho$  is kept constant in Fig. 8, this condition is inevitably violated as  $d$  becomes small, explaining the breakdown of the supergain regime.

Once (99) fails, the behavior is governed by the gap term  $\Delta_{\parallel}(d, \rho)$  in (96). Since  $\Delta_{\parallel}(d, \rho) \sim -12d \ln d$  as  $d \rightarrow 0$ , both the upper and lower bounds converge to zero, implying

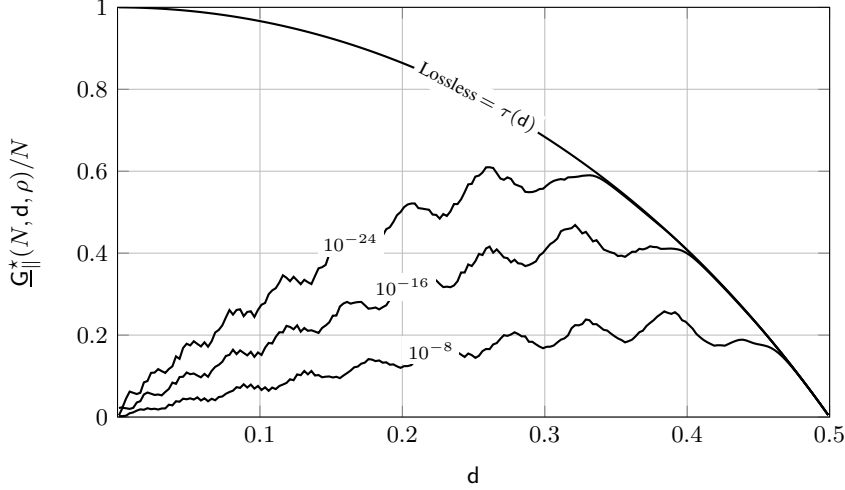


**Fig. 8:** Lower bound on the asymptotic linear scaling of the endfire supergain factor as a function of  $d$  for various  $\rho$  and  $N = 41$ . The curves are benchmarked against the lossless limit  $\tau(d)$  in (98); the linear scaling is fully exploited as  $d \rightarrow 0$  whereas it is suppressed as  $d \rightarrow 1/2$ , reflecting a progressive decrease in mutual coupling. As  $\rho$  departs from zero (with fixed  $N$  and  $d$ ), the curves deviate significantly from  $\tau(d)$ . With  $N$  and  $\rho$  fixed, the impact of losses intensifies as  $d$  decreases, violating the scaling requirement in (99).

by the squeeze theorem that the supergain factor itself vanishes. In this regime, each additional antenna introduces an exponential penalty relative to the uncoupled case. Notice how this behavior differs with that of (79) for electrically small apertures, where the supergain factor remains nonzero, also observed in [21].

## 9 Conclusion

Through a spectral analysis, this paper has characterized the fundamental limits of spatial beamforming in linear holographic arrays. The results confirm that, properly harnessed, mutual coupling arising as antenna spacing falls below a half-wavelength yields a beamforming gain that scales quadratically with the number of antennas  $N$  along the endfire direction. The price to pay for such enhancement is a gain loss everywhere else as coupling can only redistribute power across directions.

The quadratic scaling is achievable in regimes in which the coupling is strong, provided the array can withstand the reactive behavior and can sustain highly coupled modes against the backdrop of ohmic losses,  $\rho$ . Specifically:

- The spatial concentration regime (vanishing antenna spacing): As antennas collapse into a single element, coupling intensifies to an extreme degree. If losses decay at least hyperbolically with  $N$ , the gain sustains a quadratic growth; otherwise, the gain transitions to a saturation limit that scales as  $\rho^{-1}$ .

- The spectral concentration regime (increasing aperture with fixed spacing below a half wavelength): The quadratic scaling emerges not from a singular collapse, but from the cumulative contribution to mutual coupling across progressively more distant antenna pairs. To sustain this growth, the tail contributions from far-apart antennas must not saturate, ensured by  $\rho$  decaying exponentially with  $N$  for a fixed  $d$ . Further gains are achievable through array densification provided that  $\rho$  decays polynomially with  $d$ .

These findings extend beyond holographic arrays to arrays that minimize mutual coupling—such as half-wavelength spaced arrays—in wideband scenarios. Because such configuration is tailored to a center frequency, variations across the bandwidth perturb the condition, thereby activating the spectral concentration mechanisms described above [22]. As  $N$  increases, these deviations accumulate, producing non-negligible tail contributions to mutual coupling whose impact on beamforming remains unexplored.

Mutual coupling further intensifies for large apertures, off-broadside beamforming, and wideband operation, which are also the regimes where beam-squint effects become most pronounced [42]. Since both phenomena arise under the same conditions and introduce frequency-dependent distortions of the array response, their interplay warrants further investigation.

## Acknowledgment

Work supported by MICIU under the Maria de Maeztu Units of Excellence Programme (CEX2021-001195-M), and by AGAUR (Catalan Government).

## Appendix A

Let  $\mathcal{A} \subseteq \mathcal{L}^2 \left[-\frac{1}{2}, \frac{1}{2}\right]$  denote the subset of periodic spectral functions of unit period that are square-integrable over one period. The respective spectra are bandlimited to  $[-d, d]$ , each generated by a unit-norm indexlimited sequence. The problem

$$\arg \inf_{\mathcal{X}_M \subseteq \mathcal{L}^2 \left[-\frac{1}{2}, \frac{1}{2}\right]} \sup_{J \in \mathcal{A}} \inf_{\{J_k\}_{k=0}^{M-1}} \left\| J - \sum_{k=0}^{M-1} J_k U_k \right\|_{[-d, d]} \quad (\text{A1})$$

identifies the optimal  $M$ -dimensional subspace

$$\mathcal{X}_M = \text{span}(U_0, \dots, U_{M-1}), \quad (\text{A2})$$

which minimizes the worst-case approximation error in (48) of  $\mathcal{X}_M$  from  $J \in \mathcal{A}$ , by means of linear combinations of the basis functions  $\{U_k\}$  with coefficients  $\{J_k\}$  within the spectral support  $[-d, d]$ . (The normalization of the coefficients is specified later, as it hinges on that of the basis functions). Subsuming the spectral support and expressing  $J$  via (2) gives

$$\arg \inf_{\mathcal{X}_M \subseteq \mathcal{L}^2 \left[-\frac{1}{2}, \frac{1}{2}\right]} \sup_{J \in \mathcal{A}} \inf_{\{J_k\}_{k=0}^{M-1}} \left\| \mathbb{1}_{[-d, d]}(f) J - \sum_{k=0}^{M-1} J_k \mathbb{1}_{[-d, d]}(f) U_k \right\| \quad (\text{A3})$$

$$= \arg \inf_{\mathcal{X}_M \subseteq \mathcal{L}^2[-\frac{1}{2}, \frac{1}{2}]} \sup_{J \in \mathcal{A}} \inf_{\{J_k\}_{k=0}^{M-1}} \left\| \mathbb{1}_{[-d, d]}(\mathbf{f}) F I_N j_n - \sum_{k=0}^{M-1} J_k \mathbb{1}_{[-d, d]}(\mathbf{f}) U_k \right\|.$$

Recalling the operators  $B_d$  and  $I_N$  in Definition 1, let us denote the Hilbert-Schmidt operator

$$K_N = F B_d I_N, \quad (\text{A4})$$

which indexlimits a sequence to  $[N]$  and then bandlimits its spatial spectrum to  $[-d, d]$ . Further letting  $\mathcal{A} = \text{Im}(K_N) = \{K_N j_n : \|j_n\| = 1\}$  be the image of unit-norm sequences induced by the operator  $K_N$ , (A3) becomes

$$\arg \inf_{\mathcal{X}_M \subseteq \mathcal{L}^2[-\frac{1}{2}, \frac{1}{2}]} \sup_{\|j_n\|=1} \inf_{J_M \in \mathcal{X}_M} \|K_N j_n - J_M\| \quad (\text{A5})$$

where  $J_M(\mathbf{f}) = \sum_{k=0}^{M-1} J_k \mathbb{1}_{[-d, d]}(\mathbf{f}) U_k(\mathbf{f})$  and the dependence on coefficients is absorbed into the subspace  $\mathcal{X}_M$ . Introducing the adjoint operator of  $K_N$ ,

$$K_N^\dagger = I_N B_d F^{-1}, \quad (\text{A6})$$

the optimal basis  $\{U_k\}$  in (A2) according to the criterion (A5) satisfies [37, Sec. 3.4]

$$K_N K_N^\dagger U_k(\mathbf{f}) = \mu_k U_k(\mathbf{f}) \quad |\mathbf{f}| \leq d. \quad (\text{A7})$$

Expanding  $K_N K_N^\dagger$  using (A4) and (A6), and applying (21), leads to (50).

## Appendix B

The dependence of every variable on  $d$  and  $N$  is henceforth omitted as they are kept fixed throughout. Let us rewrite (62) compactly as

$$J(\mathbf{f}) = \boldsymbol{\nu}^T(\mathbf{f}) \mathbf{i} \quad (\text{B8})$$

with  $[\boldsymbol{\nu}(\mathbf{f})]_k = U_k(\mathbf{f})$  and  $[\mathbf{i}]_k = J_k$  the  $k$ th spectral basis function and corresponding expansion coefficient, for  $k = 0, \dots, N-1$ . Under this mapping, the normalization condition in (64) implies  $\|\mathbf{i}\| = 1$ . Squaring the absolute value of (B8) and averaging over  $[-d, d]$ ,

$$\frac{1}{2d} \int_{-d}^d |J(\mathbf{g})|^2 d\mathbf{g} = \mathbf{i}^H \left( \frac{1}{2d} \int_{-d}^d \boldsymbol{\nu}(\mathbf{g}) \boldsymbol{\nu}^T(\mathbf{g}) d\mathbf{g} \right) \mathbf{i} \quad (\text{B9})$$

$$= \mathbf{i}^H \boldsymbol{\Lambda} \mathbf{i}, \quad (\text{B10})$$

where  $\boldsymbol{\Lambda} = \text{diag}(\lambda_0, \dots, \lambda_{N-1})$ , with  $\lambda_k > 0$  the eigenvalues of  $\mathbf{C}$  in (26). The above equation follows from the orthogonality of the  $U_k$ 's in (59) and the coupling-prolate identity

in (72). Substituting the square value of (B8) and (B10) respectively into the numerator and denominator of (11), the array gain function equals

$$G(\rho, \mathbf{i}, \mathbf{f}) = \frac{|\boldsymbol{\nu}(\mathbf{f})^\top \mathbf{i}|^2}{\mathbf{i}^\text{H} \Lambda(\rho) \mathbf{i}}, \quad (\text{B11})$$

where  $\Lambda(\rho) = \mathbf{\Lambda} + \rho \mathbf{I}_N$  is diagonal with its entries being the ordered eigenvalues of  $\mathbf{C}(\rho)$  in (27). Similarly, the  $Q$  factor in (12) is derived using (B10) as

$$Q(\rho, \mathbf{i}) = (\mathbf{i}^\text{H} \Lambda(\rho) \mathbf{i})^{-1}. \quad (\text{B12})$$

(The dependence of  $G(\rho, \mathbf{i}, \mathbf{f})$  and  $Q(\rho, \mathbf{i})$  on the spectrum  $J(\mathbf{f})$  is encoded into  $\mathbf{i}$ .) The maximum of (B11) at any  $\mathbf{f}'$  is obtained by solving the generalized Rayleigh quotient

$$\underset{\mathbf{i}: \|\mathbf{i}\|=1}{\text{maximize}} \quad \frac{\mathbf{i}^\text{H} \mathbf{N}(\mathbf{f}') \mathbf{i}}{\mathbf{i}^\text{H} \Lambda(\rho) \mathbf{i}}, \quad (\text{B13})$$

where  $\mathbf{N} = \boldsymbol{\nu} \boldsymbol{\nu}^\top$  is a unit-rank matrix. Following the same steps that lead from (31) to (34), the maximizer of (B13) is the unique vector of spectral coefficients

$$\mathbf{i}^*(\rho, \mathbf{f}') = \frac{\Lambda(\rho)^{-1} \boldsymbol{\nu}(\mathbf{f}')}{\|\Lambda(\rho)^{-1} \boldsymbol{\nu}(\mathbf{f}')\|} \quad (\text{B14})$$

with spectrum, according to (B8),

$$J^*(\mathbf{f}) = \boldsymbol{\nu}^\top(\mathbf{f}) \mathbf{i}^*(\rho, \mathbf{f}') = \frac{\boldsymbol{\nu}^\top(\mathbf{f}) \Lambda(\rho)^{-1} \boldsymbol{\nu}(\mathbf{f}')}{\|\Lambda(\rho)^{-1} \boldsymbol{\nu}(\mathbf{f}')\|}. \quad (\text{B15})$$

(Equivalently, from (B13), changing variables according to  $\mathbf{j} = \Lambda^{1/2}(\rho) \mathbf{i}$ , yields a Rayleigh quotient optimization as in (16), solved via Cauchy–Schwarz inequality.) As per (29), the supergain is obtained by substituting (B14) into (B11) and dividing by  $N$ , i.e.,

$$G^*(\rho, \mathbf{f}') = \frac{1}{N} \boldsymbol{\nu}(\mathbf{f}')^\top \Lambda(\rho)^{-1} \boldsymbol{\nu}(\mathbf{f}'). \quad (\text{B16})$$

The  $Q$  factor associated with the optimized current (B14) is then

$$Q^*(\rho, \mathbf{f}') = \frac{\|\Lambda(\rho)^{-1} \boldsymbol{\nu}(\mathbf{f}')\|^2}{\boldsymbol{\nu}(\mathbf{f}')^\top \Lambda(\rho)^{-1} \boldsymbol{\nu}(\mathbf{f}')}. \quad (\text{B17})$$

Expanding (B16), (B17), and (B15) gives the expressions in (65), (66), and (69) respectively.

## Appendix C

Expanding the derivatives in (52) leads to

$$\frac{1}{(2\pi)^2} (\cos(2\pi f) - \cos(2\pi d)) \frac{d^2 U(f)}{df^2} - \frac{1}{2\pi} \sin(2\pi f) \frac{dU(f)}{df} + \left( \frac{N^2 - 1}{4} \cos(2\pi f) - \theta \right) U(f) = 0. \quad (\text{C18})$$

Let us focus on the visible region  $|f| \leq d$  and make the dependence of  $f$  on  $d$  explicit by introducing the normalized variable

$$y = f/d \quad V(y) = U(fd) \quad (\text{C19})$$

such that  $|y| \leq 1$ . Applying the chain rule,  $\frac{d}{df} = \frac{1}{d} \frac{d}{dy}$  and  $\frac{d^2}{df^2} = \frac{1}{d^2} \frac{d^2}{dy^2}$ , (C18) becomes

$$\frac{1}{(2\pi d)^2} (\cos(2\pi yd) - \cos(2\pi d)) \frac{d^2 V(y)}{dy^2} - \frac{1}{2\pi d} \sin(2\pi yd) \frac{dV(y)}{dy} + \left( \frac{N^2 - 1}{4} \cos(2\pi yd) - \theta \right) V(y) = 0. \quad (\text{C20})$$

For small  $d$ , the expansions  $\cos x = 1 - x^2/2 + \mathcal{O}(x^4)$  and  $\sin x = x + \mathcal{O}(x^3)$  yield

$$\cos(2\pi yd) - \cos(2\pi d) = 2(\pi d)^2 (1 - y^2) + \mathcal{O}(d^4) \quad (\text{C21})$$

$$\cos(2\pi yd) = 1 + \mathcal{O}(d^2) \quad (\text{C22})$$

$$\sin(2\pi yd) = 2\pi yd + \mathcal{O}(d^3). \quad (\text{C23})$$

Substituting into (C20) and collecting leading-order terms on the left-hand side gives

$$\frac{1 - y^2}{2} \frac{d^2 V(y)}{dy^2} - y \frac{dV(y)}{dy} + \left( \frac{N^2 - 1}{4} - \theta \right) V(y) = \mathcal{O}(d^2) \quad d \rightarrow 0. \quad (\text{C24})$$

Letting  $\xi = 2\theta - \frac{N^2 - 1}{2}$ , (C24) can be written, up to a correction order of  $\mathcal{O}(d^2)$ , as the eigenvalue problem  $L_P V = \xi V$  induced by the operator

$$L_P = \frac{d}{dy} \left\{ (1 - y^2) \frac{d}{dy} \right\}. \quad (\text{C25})$$

This operator admits a complete set of real eigenfunctions in  $\mathcal{L}^2[-1, 1]$  associated with a discrete set of real positive values of  $\xi$ , namely [40, Eq. 22.6.1]

$$\xi_k = -k(k + 1). \quad (\text{C26})$$

In turn,  $\theta = \theta_k$ , whose expression is reported in (75) for  $k = 0, \dots, N-1$ . The corresponding eigenfunctions are asymptotically the Legendre polynomials,  $P_k(y)$ , which lead to the  $U_k(f)$  in (76) after reversing the transformation in (C19).

## Appendix D

From (76), for small  $d$  with fixed  $N$  and  $f'$ ,

$$U_k(N, d, f') \sim P_k\left(\frac{f'}{d}\right) \quad d \rightarrow 0. \quad (\text{D27})$$

Substituting into (65),

$$G^*(N, d, \rho, f') \sim \frac{1}{N} \sum_{k=0}^{N-1} \frac{1}{\lambda_k(N, d, \rho)} \left| P_k\left(\frac{f'}{d}\right) \right|^2. \quad (\text{D28})$$

From (73), with losses reintroduced as per (27), the eigenvalues asymptotically behave as

$$\lambda_k(N, d, \rho) \sim \rho + \frac{1}{2d} \int_{-d}^d \left| P_k\left(\frac{f}{d}\right) \right|^2 df \quad (\text{D29})$$

$$= \rho + \frac{1}{2} \int_{-1}^1 |P_k(y)|^2 dy \quad (\text{D30})$$

$$= \rho + \frac{1}{2k+1} \quad (\text{D31})$$

$$= \frac{2\rho k + 1}{2k+1} = a_k^{-1}(\rho) \quad d \rightarrow 0, \quad (\text{D32})$$

where the orthogonality relation in (77) was used. Substituting (D32) into (D28) gives

$$G^*(N, d, \rho, f') \sim \frac{1}{N} \sum_{k=0}^{N-1} a_k(\rho) \left| P_k\left(\frac{f'}{d}\right) \right|^2 \quad d \rightarrow 0. \quad (\text{D33})$$

### Endfire Supergain

Along the endfire direction ( $f' = \pm d$ ), using  $|P_k(\pm 1)| = 1$  into (D33),

$$G_{\parallel}^*(N, d, \rho) \sim \frac{1}{N} \sum_{k=0}^{N-1} a_k(\rho) \quad d \rightarrow 0. \quad (\text{D34})$$

For  $N\rho \ll 1$ , the Taylor expansion  $(1+x)^{-1} = 1 - x + \mathcal{O}(x^2)$  yields

$$a_k(\rho) = (2k+1) (1 - 2\rho k + \mathcal{O}((\rho N)^2)) \quad (\text{D35})$$

as  $k$  increases. Also,

$$\sum_{k=0}^{N-1} (2k+1) = N + 2 \sum_{k=0}^{N-1} k = N + N(N-1) = N^2 \quad (\text{D36})$$

$$\sum_{k=0}^{N-1} 2k^2 + k = \frac{1}{2}N(N-1) + \frac{1}{3}N(N-1)(2N-1) = \frac{1}{6}N(N-1)(4N+1), \quad (\text{D37})$$

after using the identities  $\sum_{k=1}^K k = K(K+1)/2$  and  $\sum_{k=1}^K k^2 = K(K+1)(2K+1)/6$  [43, Eq. 0.12]. Plugging (D35) into (D34) with (D36) and (D37) leads to (78).

Conversely, for  $N\rho \gg 1$ , grouping leading-order terms in (D34) leads to

$$a_k(\rho) = \frac{1}{\rho} \left(1 + \frac{1}{2k}\right) \left(1 + \frac{1}{2\rho k}\right)^{-1}. \quad (\text{D38})$$

As  $k$  increases, the Taylor expansion  $(1+x)^{-1} = 1 - x + \mathcal{O}(x^2)$  applied to (D38) yields

$$a_k(\rho) = \frac{1}{\rho} \left(1 + \frac{1}{2k}\right) \left(1 - \frac{1}{2\rho k} + \mathcal{O}((\rho N)^{-2})\right) \quad (\text{D39})$$

$$= \frac{1}{\rho} \left(1 - \frac{1-\rho}{2\rho k} + \mathcal{O}((\rho N)^{-2})\right), \quad (\text{D40})$$

where second-order terms were subsumed into  $\mathcal{O}((\rho N)^{-2})$ . From (D34), it holds that

$$\mathbf{G}_{\parallel}^*(N, \mathbf{d}, \rho) \sim \frac{1}{N} \left(1 + \frac{1}{\rho} \sum_{k=1}^{N-1} \left(1 - \frac{1-\rho}{2\rho k} + \mathcal{O}((\rho N)^{-2})\right)\right) \quad (\text{D41})$$

$$= \frac{1}{N} + \frac{N-1}{\rho N} - \frac{1-\rho}{\rho} \frac{1}{2\rho N} \sum_{k=1}^{N-1} \frac{1}{k} + \mathcal{O}((\rho N)^{-2}) \quad (\text{D42})$$

$$= \frac{1}{N} + \frac{N-1}{\rho N} - \frac{1-\rho}{\rho} \frac{1}{2\rho N} H_{N-1} + \mathcal{O}((\rho N)^{-2}) \quad (\text{D43})$$

with  $H_\ell$  the harmonic number of order  $\ell$ . For large  $N$  and  $N\rho \gg 1$ , using  $H_\ell = \ln \ell + \mathcal{O}(1)$  for growing  $\ell$ , (D43) leads to (79).

## Broadside Supergain

Along the broadside direction ( $f' = 0$ ), only polynomials with even indices contribute to (D33) due to the antisymmetry of  $P_k(x)$  for  $k$  odd, yielding

$$\mathbf{G}_{\perp}^*(N, \mathbf{d}, \rho) \sim \frac{1}{N} \sum_{n=0}^{\lfloor \frac{N-1}{2} \rfloor} \frac{4n+1}{4\rho n+1} |P_{2n}(0)|^2 \quad \mathbf{d} \rightarrow 0. \quad (\text{D44})$$

Let us invoke the approximation of  $P_k(x)$  with  $x = \cos \theta$ , for  $0 < \theta < \pi$  [43, Eq. 8.918]

$$P_k(\cos \theta) = \sqrt{\frac{2}{\pi k \sin(\theta)}} \cos \left[ \left( k + \frac{1}{2} \right) \theta - \frac{\pi}{4} \right] + \mathcal{O}(k^{-3/2}). \quad (\text{D45})$$

Specialized to  $\theta = \pi/2$  and  $k = 2n$ , (D45) reads as

$$P_{2n}(0) = \sqrt{\frac{1}{\pi n}} (-1)^n + \mathcal{O}(n^{-3/2}). \quad (\text{D46})$$

Using (D46) into (D44) gives, for large  $N$ ,

$$G_{\perp}^*(N, d, \rho) \sim \frac{1}{N} \left( 1 + \sum_{n=1}^{\lfloor \frac{N-1}{2} \rfloor} \frac{4n+1}{4\rho n+1} \frac{1}{\pi n} \right) \quad d \rightarrow 0. \quad (\text{D47})$$

Setting  $\rho = 0$ , (D47) specializes to

$$D_{\perp}^*(N, d) \sim \frac{1}{N} \left( 1 + \frac{4}{\pi} \sum_{n=1}^{\lfloor \frac{N-1}{2} \rfloor} \left( 1 + \frac{1}{4n} \right) \right) \quad (\text{D48})$$

$$= \frac{1}{N} \left( 1 + \frac{4}{\pi} \left[ \frac{N-1}{2} \right] + \frac{1}{\pi} H_{\lfloor \frac{N-1}{2} \rfloor} \right) \quad d \rightarrow 0, \quad (\text{D49})$$

where, recall,  $H_{\ell}$  is the harmonic number. Thus, for large  $N$ , (D48) becomes

$$D_{\perp}^*(N, d) \sim \frac{4}{\pi N} \left[ \frac{N}{2} \right] + \frac{1}{\pi N} \ln \left[ \frac{N}{2} \right] + \mathcal{O}(N^{-1}) \quad d \rightarrow 0. \quad (\text{D50})$$

where  $H_{\ell} = \ln \ell + \mathcal{O}(1)$  was used again. Relaxing the rounding operation, which produces  $\mathcal{O}(1)$  corrections for any  $N$ , and retaining only leading terms as  $N$  grows, the behavior is obtained.

## Appendix E

To facilitate the analysis near the endfire direction,  $f = d$ , let us introduce the transformation

$$u = \cos(2\pi f) - A \quad (\text{E51})$$

as well as

$$\Xi_k(N, d, u) = U_k \left( N, d, \arccos \left( \frac{u+A}{2\pi} \right) \right), \quad (\text{E52})$$

where  $A$  is defined in (52) and  $u$  is nonnegative in the visible region  $\{0 \leq f \leq d\}$ . Because the asymptotic parameters  $B$  and  $C$  are uniquely specified within each subset  $\mathcal{K}_i$ , any notational ambiguity is naturally resolved by the context of the subset being analyzed.

## E.1 Asymptotic Analysis

**Low-pass region:**  $-1 < A < B < 1$  or  $\mathcal{K}_1 = \{k = \lfloor N_0(1 - x_1) \rfloor, 0 < x_1 < 1\}$

Specializing the asymptotic constraint in (88) to  $k \in \mathcal{K}_1$  and omitting rounding errors, which only produce  $\mathcal{O}(1/N)$  corrections for large  $N$ ,

$$B(\mathbf{d}, x_1) = \left\{ A < B < 1 : \int_B^1 \sqrt{\frac{t-B}{(t-A)(1-t^2)}} dt \sim 2\pi d(1-x_1) \right\}, \quad (\text{E53})$$

where  $N_0 = 2dN$  was used. Let us introduce the positive integrals [32, Eq. 47]

$$\begin{aligned} L_1(\mathbf{d}, B) &= \int_B^1 R(\mathbf{d}, B, t) dt & L_2(\mathbf{d}, B) &= \int_B^1 S(\mathbf{d}, B, t) dt \\ L_3(\mathbf{d}, B) &= \int_A^B R(\mathbf{d}, B, t) dt & L_4(\mathbf{d}, B) &= \int_A^B S(\mathbf{d}, B, t) dt, \end{aligned} \quad (\text{E54})$$

where

$$\begin{aligned} R(\mathbf{d}, B, t) &= \left| \frac{t-B}{(t-A)(1-t^2)} \right|^{1/2} \\ S(\mathbf{d}, B, t) &= |(t-B)(t-A)(1-t^2)|^{-1/2}. \end{aligned} \quad (\text{E55})$$

For any  $\mathbf{d}$ , each integral is an implicit function of the asymptotic parameter  $x_1$  via  $B$  through the constraint (E53). This dependence is henceforth subsumed into that of  $x_1$  by defining

$$L_i(\mathbf{d}, x_1) = L_i(\mathbf{d}, B(\mathbf{d}, x_1)), \quad i = 1, 2, 3. \quad (\text{E56})$$

For any admissible  $x_1$ , further define [32, Eqs. 43, 45]

$$C(\mathbf{d}, x_1) = \frac{4}{L_2(\mathbf{d}, x_1)} \left[ \frac{N}{2} L_1(\mathbf{d}, x_1) + \left( 2 + (-1)^{\lfloor 2dN(1-x_1) \rfloor} \right) \frac{\pi}{4} \right]_{\text{rem } 2\pi}. \quad (\text{E57})$$

For large  $N$ , the eigenfunctions expand as [32, Eq. 42]

$$|\Xi_k(N, \mathbf{d}, \mathbf{u})| \sim |d_1(N, \mathbf{d}, x_1)| I_0 \left( N \sqrt{\frac{B-A}{1-A^2}} \mathbf{u} \right) \quad N \rightarrow \infty, \quad (\text{E58})$$

where  $I_0(\cdot)$  is the modified Bessel function of the first kind, and

$$|d_1(N, \mathbf{d}, x_1)| = \pi \sqrt{\frac{N e^{-C(\mathbf{d}, x_1) L_4(\mathbf{d}, x_1)/2} e^{-N L_3(\mathbf{d}, x_1)}}{L_2(\mathbf{d}, x_1) \sqrt{1-A^2}}}. \quad (\text{E59})$$

Since  $I_0(\mathbf{u}) \sim 1$  for  $\mathbf{u} \rightarrow 0$ , near the endfire direction

$$|\Xi_k(N, \mathbf{d}, \mathbf{u})|^2 \sim |\Xi_{\parallel}^{(1)}(N, \mathbf{d}, x_1)|^2 \quad (\text{E60})$$

$$= \frac{\pi^2 e^{-C(d,x_1)L_4(d,x_1)/2}}{L_2(d,x_1)\sqrt{1-A^2}} N e^{-L_3(d,x_1)N} \quad \mathbf{u} \rightarrow 0, N \rightarrow \infty.$$

The corresponding eigenvalues converge to unity exponentially fast with increasing  $N$ , i.e.,

$$1 - \mu_k(N, \mathbf{d}) \sim 1 - \mu^{(1)}(N, \mathbf{d}, x_1) = e^{-C(d,x_1)L_4(d,x_1)/2} e^{-L_3(d,x_1)N} \quad N \rightarrow \infty. \quad (\text{E61})$$

**All-pass region:**

$$-1 < A = B < 1 \text{ or } \mathcal{K}_2 = \{k = \lfloor N_0 + \frac{x_2}{\pi} \log(N) \rfloor, -\frac{\pi N_0}{\log(N)} < x_2 < \frac{\pi}{\log(N)}(N - N_0)\}$$

Near  $B = A$ , specifically for  $0 \leq \mathbf{u} \leq N^{-2/3}$ , we have that [32, Eq. 50]

$$|\Xi_k(N, \mathbf{d}, \mathbf{u})| \sim |e_2(N, \mathbf{d}, x_2)| \left| \Phi\left(\frac{1}{2} - j\frac{E(N, \mathbf{d}, x_2)\beta}{2}, 1; -j\beta N \mathbf{u}\right) \right| \quad N \rightarrow \infty, \quad (\text{E62})$$

where  $\beta = (1 - A^2)^{-1/2} = |\csc(2\pi \mathbf{d})|$  and  $\Phi(\cdot)$  is the confluent hypergeometric function. The normalization constant is

$$|e_2(N, \mathbf{d}, x_2)| = r(E(N, \mathbf{d}, x_2)\beta) e^{\frac{\pi}{4}E(N, \mathbf{d}, x_2)\beta} |e_1(N, \mathbf{d}, x_2)| N^{1/2}, \quad (\text{E63})$$

with

$$|e_1(N, \mathbf{d}, x_2)| = \sqrt{\frac{3\pi}{(1 + e^{\pi E(N, \mathbf{d}, x_2)\beta}) \log N}}. \quad (\text{E64})$$

$E(N, \mathbf{d}, x_2)$  is determined as the absolute value of the smallest root of [32, Eq. 53] with the index  $k$  in the formulation specialized to the subset  $\mathcal{K}_2$ ,

$$\frac{E\beta - x_2}{2} \log N = \frac{E\beta}{2} \log \frac{\beta}{2} - \psi(E\beta) = \mathcal{O}(1). \quad (\text{E65})$$

In turn,  $r(s) = |\Gamma(\frac{1}{2} - \frac{1}{2}js)|$  and  $\psi(s) = \arg(\Gamma(\frac{1}{2} - \frac{1}{2}js))$  with  $\Gamma(\cdot)$  the Gamma function. Thus, to leading order,

$$E(N, \mathbf{d}, x_2)\beta = x_2 + \mathcal{O}\left(\frac{1}{\log N}\right) \quad N \rightarrow \infty. \quad (\text{E66})$$

Using the identity  $|\Gamma(\frac{1}{2} + jy)|^2 = \pi \cosh^{-1}(\pi y)$  [40, Eq. 6.1.30], the term (which follows from the continuity of the limit)

$$r(E(N, \mathbf{d}, x_2)\beta) \sim \sqrt{\pi} \cosh^{-1/2}\left(\frac{\pi x_2}{2}\right) \quad N \rightarrow \infty \quad (\text{E67})$$

yields

$$|e_2(N, \mathbf{d}, x_2)| \sim \pi \cosh^{-1/2}\left(\frac{\pi x_2}{2}\right) e^{\pi x_2/4} \sqrt{\frac{3}{1 + e^{\pi x_2}}} \sqrt{\frac{N}{\log N}} \quad N \rightarrow \infty. \quad (\text{E68})$$

Substituting into (E62) and using  $\Phi(a, c; -jz) \sim 1$  for  $z = \beta N u \ll 1$ , in the region  $u \ll N^{-1}$  we have that

$$\begin{aligned} |\Xi_k(N, \mathbf{d}, x_2, \mathbf{u})|^2 &\sim |\Xi_{\parallel}^{(2)}(N, \mathbf{d}, x_2)|^2 \\ &= \frac{3\pi^2 e^{\pi x_2/2}}{\cosh(\frac{\pi x_2}{2})(1 + e^{\pi x_2})} \frac{N}{\log N} \quad \mathbf{u} \rightarrow 0, N \rightarrow \infty. \end{aligned} \quad (\text{E69})$$

The corresponding eigenvalues exhibit a smooth transition from 1 to 0 as the parameter  $x_2$  spans its entire domain, asymptotically giving

$$\mu_k(N, \mathbf{d}) \sim \mu^{(2)}(N, \mathbf{d}, x_2) = (1 + e^{\pi x_2})^{-1} \quad N \rightarrow \infty. \quad (\text{E70})$$

**High-pass region:**  $-1 < A' < B < 1$  or  $\mathcal{K}_3 = \{k = \lfloor N_0(1 + x_3) \rfloor, 0 < x_3 < \frac{1}{2d} - 1\}$

Capitalizing on spectral symmetry, let us introduce the auxiliary variables [32, Eqs. 56-57]

$$f' = \frac{1}{2} - f \quad d' = \frac{1}{2} - d \quad k' = N - 1 - k, \quad (\text{E71})$$

such that  $A' = \cos(2\pi d') = -A$ . From  $k \in \mathcal{K}_3$ ,

$$k' \sim 2d'N(1 - x'_3) \quad x'_3 \sim \frac{d}{d'}x_3, \quad (\text{E72})$$

where  $0 < x_3 < d'/d$  ensuring  $0 < x'_3 < 1$ .

Applying the substitution  $s = \cos(2\pi f') = -t$  and expressing  $k$  in terms of  $k'$  via the asymptotic identity  $k + k' \sim N$ , the constraint in (88) specializes for  $k \in \mathcal{K}_3$  to

$$B(\mathbf{d}, x'_3) = \left\{ A' < B < 1 : \int_{-1}^{-B} \sqrt{\frac{s+B}{(s+A')(1-s^2)}} ds \sim 2\pi d'(1-x'_3) \right\}, \quad (\text{E73})$$

where the relationship  $\sim$  arises from the asymptotic behavior of  $k'$  in (E72). Due to symmetry, the positive integrals in (E54) morph into

$$\begin{aligned} L'_1(\mathbf{d}, B) &= \int_{-1}^{-B} R'(\mathbf{d}, B, s) ds & L'_2(\mathbf{d}, B) &= \int_{-1}^{-B} S'(\mathbf{d}, B, s) ds \\ L'_3(\mathbf{d}, B) &= \int_{-B}^{-A'} R'(\mathbf{d}, B, s) ds & L'_4(\mathbf{d}, B) &= \int_{-B}^{-A'} S'(\mathbf{d}, B, s) ds, \end{aligned} \quad (\text{E74})$$

where

$$\begin{aligned} R'(\mathbf{d}, B, s) &= \left| \frac{s+B}{(s+A')(1-s^2)} \right|^{1/2} \\ S'(\mathbf{d}, B, s) &= |(s+B)(s+A')(1-s^2)|^{-1/2}. \end{aligned} \quad (\text{E75})$$

Due to the symmetry,  $|U_k(N, \mathbf{d}, \mathbf{f})| = |U_{k'}(N, \mathbf{d}', \mathbf{f}')|$ , yielding, for large  $N$ , [32, Eq. 42]

$$|\Xi_k(N, \mathbf{d}, \mathbf{u}')| \sim |d_3(N, \mathbf{d}, x'_3)| J_0 \left( N \sqrt{\frac{B - A'}{1 - (A')^2}} u' \right), \quad (\text{E76})$$

where  $d_3$  follows from  $d_1$  in (E59) upon replacing the  $L_i$ 's by their counterparts  $L'_i$ 's, and replacing  $C$  in (E57) by

$$C(\mathbf{d}', x'_3) = \frac{4}{L'_2(\mathbf{d}', x'_3)} \left[ \frac{N}{2} L'_1(\mathbf{d}', x'_3) + \left( 2 + (-1)^{\lfloor 2d'N(1-x'_3) \rfloor} \right) \frac{\pi}{4} \right]_{\text{rem } 2\pi}. \quad (\text{E77})$$

Accordingly, since  $J_0(u') \sim 1$  for  $u' \rightarrow 0$ , the eigenfunctions squared behave as

$$\begin{aligned} \left| \Xi_k(N, \mathbf{d}, x'_3, \mathbf{u}') \right|^2 &\sim \left| \Xi_{\parallel}^{(3)}(N, \mathbf{d}, x'_3) \right|^2 \\ &= \frac{\pi^2 e^{-C(\mathbf{d}, x'_3) L'_4(\mathbf{d}, x'_3)/2}}{L'_2(\mathbf{d}, x'_3) \sqrt{1 - (A')^2}} N e^{-L'_3(\mathbf{d}, x'_3) N} \quad \mathbf{u}' \rightarrow 0, N \rightarrow \infty. \end{aligned} \quad (\text{E78})$$

Due to symmetry,  $\mu_k(N, \mathbf{d}) = 1 - \mu_{k'}(N, \mathbf{d}')$ , implying from (E61) that the eigenvalues decay exponentially fast with increasing  $N$ ,

$$\mu_k(N, \mathbf{d}) \sim \mu^{(3)}(N, \mathbf{d}, x'_3) = e^{-C(\mathbf{d}', x'_3) L'_4(\mathbf{d}', x'_3)/2} e^{-L'_3(\mathbf{d}', x'_3) N} \quad N \rightarrow \infty. \quad (\text{E79})$$

## E.2 Removal of Singularities in the $L$ Integrals

The integrals defined by  $L_i(\mathbf{d}, B)$  in (E54) and  $L'_i(\mathbf{d}, B)$  in (E74) exhibit endpoint singularities. Let us focus on the latter family of integrals, which governs the asymptotic behavior within  $\mathcal{K}_3$  in the analysis of Appendix F, that is

$$L'_i(\mathbf{d}, B) = \int_{s_L}^{s_U} \ell'_i(\mathbf{d}, B, s) ds \quad -1 \leq s_L < s_U < 1, \quad (\text{E80})$$

where the kernel  $\ell'_i(\mathbf{d}, B, s)$  is either  $R'(\mathbf{d}, B, s)$  or  $S'(\mathbf{d}, B, s)$ , both being defined in (E75). Letting  $\mathcal{P}_i(f)$  be the set of simple poles for a kernel  $f(s)$  within  $\ell'_i$ ,

$$\mathcal{P}_i(R') = \begin{cases} \{-1\} & i = 1 \\ \{-A'\} & i = 3 \end{cases} \quad \mathcal{P}_i(S') = \begin{cases} \{-B, -1\} & i = 2 \\ \{-B, -A'\} & i = 4. \end{cases} \quad (\text{E81})$$

To resolve the singularities, the change of variables  $\phi \rightarrow s$  is applied, whereby

$$s = s_L + (s_U - s_L) \sin^2 \phi \quad ds = 2(s_U - s_L) \sin \phi \cos \phi d\phi. \quad (\text{E82})$$

The resulting differential cancels the singularities, yielding the regularized integrals in (91).

### E.3 Existence and Uniqueness of the Mapping $x'_3 \rightarrow B$ in (E73)

The asymptotic constraint in (E73) bounds  $B(d, x'_3)$  within  $A' < B < 1$ . This is consistent with the limits of the parameter  $0 < x'_3 < 1$ , as inferred from the boundary behaviors

$$\lim_{B \rightarrow 1} \int_{-1}^{-B} \sqrt{\frac{s+B}{(s+A')(1-s^2)}} ds = \int_0^{\pi/2} \frac{0}{2\sqrt{1+A}} d\phi = 0 \quad (\text{E83})$$

$$\lim_{B \rightarrow A'} \int_{-1}^{-B} \sqrt{\frac{s+B}{(s+A')(1-s^2)}} ds = \int_{-1}^{-A'} \frac{ds}{\sqrt{1-s^2}} = \arccos(A') = 2\pi d', \quad (\text{E84})$$

where the transformation in (E82) was used. These integrals ensure that  $x'_3$  fully spans the domain of  $B$  through the limits  $x'_3 \rightarrow 1$  and  $x'_3 \rightarrow 0$  applied to (E73). Further applying the Leibniz integral rule to differentiate the integral of (E73) with respect to  $B$ ,

$$\frac{d}{dB} \int_{-1}^{-B} \sqrt{\frac{s+B}{(s+A')(1-s^2)}} ds = \int_{-1}^{-B} \left| \frac{1}{(s+A')(1-s^2)} \right|^{1/2} \frac{s+B}{2|s+B|^{3/2}} ds. \quad (\text{E85})$$

Since  $s < -B$  throughout the integration interval, the term  $s+B$  is negative whereas the remaining terms are positive, implying that the integral is monotonically decreasing with respect to  $B$ . Differentiating both sides of the constraint in (E73) via the chain rule yields

$$\frac{dB}{dx'_3} \sim -(2\pi d') \left( \frac{d}{dB} \int_{-1}^{-B} \sqrt{\frac{s+B}{(s+A')(1-s^2)}} ds \right)^{-1}, \quad (\text{E86})$$

which is positive, as the integral's derivative is negative. This monotonicity dictates that the mapping  $x'_3 \rightarrow B$  is injective. Combined with the surjectivity established by the boundary limits in (E83), the inverse mapping exists and is unique (see Fig. 5). This invertibility allows the auxiliary integrals  $L'_i(d, B)$  to be expressed directly in terms of the parameter  $x'_3$  via

$$L'_i(d, x'_3) = L'_i(d, B(d, x'_3)) \quad i = 1, 2, 3. \quad (\text{E87})$$

## Appendix F

By applying (E51) and combining (27) with (72), the endfire supergain in (65) can be expressed as a sum of positive terms over the index set  $\mathcal{K} = \{0, \dots, N-1\}$ , namely

$$G_{\parallel}^*(N, d, \rho) = \frac{1}{N} \sum_{k \in \mathcal{K}} r_k^{(i)}(N, d, \rho), \quad (\text{F88})$$

where the individual contributions are defined by

$$r_k^{(i)}(N, d, \rho) = \frac{|\Xi_k(N, d, 0)|^2}{(2d)^{-1} \mu_k(N, d) + \rho}. \quad (\text{F89})$$

Define a non-disjoint cover of the set  $\mathcal{K}$  by  $\bigcup_{i=1}^3 \mathcal{K}_i = \mathcal{K}$ . These subsets satisfy  $\mathcal{K}_1 \cap \mathcal{K}_3 = \emptyset$ , while  $\mathcal{K}_2$  overlaps with both  $\mathcal{K}_1$  and  $\mathcal{K}_3$ . Let  $S_N^{(i)}(\mathbf{d}, \rho)$  be the partial sum over each subset:

$$S_N^{(i)}(\mathbf{d}, \rho) = \frac{1}{N} \sum_{k \in \mathcal{K}_i} r_k^{(i)}(N, \mathbf{d}, \rho). \quad (\text{F90})$$

As every  $r_k^{(i)}$  is positive, the partial subset overlap implies that a summation of  $S_N^{(i)}(\mathbf{d}, \rho)$  overcounts certain indices, providing an upper bound on the supergain. Conversely, considering only the region  $\mathcal{K}_3$  in isolation yields a lower bound. Altogether

$$\underline{G}_{\parallel}^*(N, \mathbf{d}, \rho) < G_{\parallel}^*(N, \mathbf{d}, \rho) < \overline{G}_{\parallel}^*(N, \mathbf{d}, \rho), \quad (\text{F91})$$

where the nonachievable bounds are

$$\overline{G}_{\parallel}^*(N, \mathbf{d}, \rho) = \sum_{i=1}^3 S_N^{(i)}(\mathbf{d}, \rho) \quad \text{and} \quad \underline{G}_{\parallel}^*(N, \mathbf{d}, \rho) = S_N^{(3)}(\mathbf{d}, \rho). \quad (\text{F92})$$

As  $N \rightarrow \infty$ , the summands within each subset  $\mathcal{K}_i$  are asymptotically described by the continuous functions  $\Xi_{\parallel}^{(i)}(N, \mathbf{d}, x_i)$  and  $\mu^{(i)}(N, \mathbf{d}, x_i)$ , replacing the dependence on the discrete index  $k \in \mathcal{K}_i$  by the continuous variables  $x_i$ . Invoking the asymptotic results from Appendix E, the ratio in (F89) converges to the continuous function

$$r^{(i)}(N, \mathbf{d}, \rho, x_i) = \frac{|\Xi_{\parallel}^{(i)}(N, \mathbf{d}, x_i)|^2}{(2\mathbf{d})^{-1} \mu^{(i)}(N, \mathbf{d}, x_i) + \rho} = \begin{cases} \frac{\pi e^{-C(\mathbf{d}, x_1) L_4(\mathbf{d}, x_1)/2} L_2(\mathbf{d}, x_1) \text{sinc}(2\mathbf{d})}{N e^{-L_3(\mathbf{d}, x_1)N}} & i = 1 \\ \frac{1 - e^{-C(\mathbf{d}, x_1) L_4(\mathbf{d}, x_1)/2} e^{-L_3(\mathbf{d}, x_1)N}}{1 + e^{\pi x_2} 1 + 2\mathbf{d}\rho} + 2\mathbf{d}\rho & \\ \frac{e^{\pi x_2}}{1 + e^{\pi x_2}} \frac{12\pi^2 \mathbf{d}}{1 + 2\mathbf{d}\rho(1 + e^{\pi x_2})} \frac{N}{\log N} & i = 2 \\ \frac{\pi N}{L_2'(\mathbf{d}, x_3') \text{sinc}(2\mathbf{d})} & \\ \frac{1}{1 + 2\mathbf{d}\rho e^{C(\mathbf{d}, x_3') L_4'(\mathbf{d}, x_3')/2} e^{L_3'(\mathbf{d}, x_3')N}} & i = 3 \end{cases} \quad (\text{F93})$$

where  $\sqrt{1 - A^2} = \sin(2\pi \mathbf{d})$  from (53) and  $2 \cosh(x) = e^x + e^{-x}$  were used.

To assess the behavior of the sums  $S_N^{(i)}(\mathbf{d}, \rho)$  as  $N \rightarrow \infty$ , each is converted to a Riemann sum and the resulting expression is replaced by the convergent integral [41, Sec. 6.7]. For each subset  $\mathcal{K}_i$ , the discrete points  $x_{i,k}$  are obtained by inverting the map  $x_i \rightarrow k$  in Appendix E while a step size  $\Delta_{x_i,k} = x_{i,k+1} - x_{i,k}$  is naturally revealed by the normalization of the supergain factor in (29).

- Subset  $\mathcal{K}_1$ : By mapping  $1 - x_{1,k} = \frac{k}{2dN}$ , the step size becomes  $\Delta_{x_{1,k}} = -\frac{1}{2dN} = \Delta_{x_1}$ . Evaluating the endpoints  $k = 0$  and  $k = \lfloor 2dN \rfloor$  maps the limits to  $x_{1,0} = 1$  and  $x_{1,\lfloor 2dN \rfloor} = 0$  (up to a vanishing error due to round-off). Since the differential vanishes asymptotically as  $N \rightarrow \infty$ , the sum (F90) for  $\mathcal{K}_1$  converges to

$$\lim_{N \rightarrow \infty} S_N^{(1)}(\mathbf{d}, \rho) = \lim_{N \rightarrow \infty} \frac{1}{N} \sum_{k \in \mathcal{K}_1} r^{(1)}(N, \mathbf{d}, \rho, x_{1,k}) \quad (\text{F94})$$

$$= 2d \lim_{\Delta_{x_1} \rightarrow 0} \sum_{k \in \mathcal{K}_1} r^{(1)}(N, \mathbf{d}, \rho, x_{1,k}) \Delta_{x_1} \quad (\text{F95})$$

$$= 2d \int_0^1 r^{(1)}(N, \mathbf{d}, \rho, x_1) dx_1, \quad (\text{F96})$$

where the minus sign in the differential cancels out by swapping integration limits.

- Subset  $\mathcal{K}_2$ : Defining  $x_{2,k} = \frac{\pi}{\log N}(k - 2dN)$ , the step size becomes  $\Delta_{x_{2,k}} = \frac{\pi}{\log N} = \Delta_{x_2}$ . The endpoints  $k = 0$  and  $k = N$  map to

$$x_{2,0} = -\frac{2\pi dN}{\log N} \quad \text{and} \quad x_{2,N} = \frac{\pi N}{\log N}(1 - 2d). \quad (\text{F97})$$

While the differential vanishes more slowly than in  $\mathcal{K}_1$ , the discrete set becomes more dense as  $N \rightarrow \infty$ . The sum in (F90) for  $\mathcal{K}_2$  behaves as

$$\lim_{N \rightarrow \infty} S_N^{(2)}(\mathbf{d}, \rho) = \lim_{N \rightarrow \infty} \frac{1}{N} \sum_{k \in \mathcal{K}_2} r^{(2)}(N, \mathbf{d}, \rho, x_{2,k}) \quad (\text{F98})$$

$$= \frac{1}{\pi} \lim_{\Delta_{x_2} \rightarrow 0} \sum_{k \in \mathcal{K}_2} \left( \frac{\log N}{N} r^{(2)}(N, \mathbf{d}, \rho, x_{2,k}) \right) \Delta_{x_2} \quad (\text{F99})$$

$$= \frac{1}{\pi} \int_{-\infty}^{\infty} \left( r^{(2)}(N, \mathbf{d}, \rho, x_2) \frac{\log N}{N} \right) dx_2, \quad (\text{F100})$$

where the integration limits tend to  $\pm\infty$  as  $N \rightarrow \infty$ . Notice how the multiplication factor suggests that the contribution vanishes, but this effect is compensated by the integrand  $r^{(2)}(N, \mathbf{d}, \rho, x_2)$  being of order  $\mathcal{O}(N/\log N)$  as per (E69), ensuring the sum remains nonzero asymptotically. Particularly, replacing  $r^{(2)}(N, \mathbf{d}, \rho, x_2)$  by (F93) yields

$$\lim_{N \rightarrow \infty} S_N^{(2)}(\mathbf{d}, \rho) = 12\pi d \int_{-\infty}^{\infty} \frac{e^{\pi x_2}}{(1 + e^{\pi x_2})(1 + 2d\rho + 2d\rho e^{\pi x_2})} dx_2 \quad (\text{F101})$$

$$= 12d \int_0^{\infty} \frac{1}{(1+u)(1+2d\rho+2d\rho u)} du \quad (\text{F102})$$

$$= 12d \int_0^{\infty} \left( \frac{1}{1+u} + \frac{2d\rho}{1+2d\rho+2d\rho u} \right) du \quad (\text{F103})$$

$$= 12d \ln \left( 1 + \frac{1}{2d\rho} \right) \quad N \rightarrow \infty, \quad (\text{F104})$$

after applying the substitution  $u = e^{\pi x_2}$  and using the partial fraction decomposition. The subset  $\mathcal{K}_2$  presents a subtle integrability issue in the lossless case ( $\rho = 0$ ) as the integrand remains flat as  $x_2 \rightarrow \infty$ . Assuming a small loss, however, integrability is restored, compounded by the exponential decay of the integrand as  $x_2 \rightarrow -\infty$ .

- Subset  $\mathcal{K}_3$ : Leveraging the spectral symmetry in (E71), let us define  $1 - x'_{3,k'} = \frac{k'}{2d'N}$  such that

$$\Delta'_{x_3,k} = -\frac{1}{2d'N} = \Delta'_{x_3}, \quad (\text{F105})$$

expressed in terms of the auxiliary variables  $k' \in \mathcal{K}_1$  and  $d'$  given in (E72). The endpoints  $k' = 0$  and  $k' = \lfloor 2d'N \rfloor$  map to  $x'_{3,0} = 1$  and  $x'_{3,\lfloor 2d'N \rfloor} = 0$  (up to a round-off error). Akin to  $\mathcal{K}_1$ , the sum in (F90) for  $\mathcal{K}_3$  converges to

$$\lim_{N \rightarrow \infty} S_N^{(3)}(\mathbf{d}, \rho) = \lim_{N \rightarrow \infty} \frac{1}{N} \sum_{k \in \mathcal{K}_3} r^{(3)}(N, \mathbf{d}, \rho, x_{3,k}) \quad (\text{F106})$$

$$= \lim_{N \rightarrow \infty} \frac{1}{N} \sum_{k' \in \mathcal{K}_1} r^{(3)}(N, \mathbf{d}, \rho, x'_{3,k'}) \quad (\text{F107})$$

$$= 2d' \lim_{\Delta'_{x_3} \rightarrow 0} \sum_{k' \in \mathcal{K}_1} r^{(3)}(N, \mathbf{d}, \rho, x'_{3,k'}) \Delta'_{x_3} \quad (\text{F108})$$

$$= 2d' \int_0^1 r^{(3)}(N, \mathbf{d}, \rho, x'_3) dx'_3, \quad (\text{F109})$$

where  $r^{(3)}(\cdot)$  inherently accounts for symmetry transformations (see Appendix E).

The upper and lower bounds for the endfire supergain are thus established by the aggregate or individual contributions of these integral approximations, for  $N \rightarrow \infty$ , as

$$\begin{aligned} \overline{\mathcal{G}}_{\parallel}^*(N, \mathbf{d}, \rho) &\sim 2d \int_0^1 r^{(1)}(N, \mathbf{d}, \rho, x_1) dx_1 + \frac{1}{\pi} \int_{-\infty}^{\infty} \left( r^{(2)}(N, \mathbf{d}, \rho, x_2) \frac{\log N}{N} \right) dx_2 \\ &\quad + 2d' \int_0^1 r^{(3)}(N, \mathbf{d}, \rho, x'_3) dx'_3 \end{aligned} \quad (\text{F110})$$

$$\underline{\mathcal{G}}_{\parallel}^*(N, \mathbf{d}, \rho) \sim 2d' \int_0^1 r^{(3)}(N, \mathbf{d}, \rho, x'_3) dx'_3. \quad (\text{F111})$$

## Appendix G

By specializing (F110) and (F111) to the zero-loss case ( $\rho = 0$ ), the superdirectivity factor is bounded as

$$\underline{\mathcal{D}}_{\parallel}^*(N, \mathbf{d}) < \mathcal{D}_{\parallel}^*(N, \mathbf{d}) < \overline{\mathcal{D}}_{\parallel}^*(N, \mathbf{d}), \quad (\text{G112})$$

where the upper bound encompasses all three index subsets,

$$\overline{\mathcal{D}}_{\parallel}^*(N, \mathbf{d}) \sim 2d \int_0^1 r^{(1)}(N, \mathbf{d}, 0, x_1) dx_1 + \frac{1}{\pi} \int_{-\infty}^{\infty} \left( r^{(2)}(N, \mathbf{d}, 0, x_2) \frac{\log(N)}{N} \right) dx_2$$

$$+ 2d' \int_0^1 r^{(3)}(N, \mathbf{d}, 0, x'_3) dx'_3 \quad N \rightarrow \infty, \quad (\text{G113})$$

and the lower bound retains only the final term,

$$\underline{D}_{\parallel}^*(N, \mathbf{d}) \sim 2d' \int_0^1 r^{(3)}(N, \mathbf{d}, 0, x'_3) dx'_3 \quad N \rightarrow \infty. \quad (\text{G114})$$

In the absence of losses, the scaled eigenvalues  $\mu^{(i)}/(2d)$  dominate the denominator of the asymptotic ratios  $r^{(i)}(N, \mathbf{d}, 0, x_i)$  in (F93), yielding

$$r^{(i)}(N, \mathbf{d}, 0, x_i) = 2d \frac{|\Xi_{\parallel}^{(i)}(N, \mathbf{d}, x_i)|^2}{\mu^{(i)}(N, \mathbf{d}, x_i)} = \begin{cases} \frac{\pi}{L_2(\mathbf{d}, x_1) \text{sinc}(2d)} \frac{N}{e^{C(\mathbf{d}, x_1) L_4(\mathbf{d}, x_1)/2} e^{L_3(\mathbf{d}, x_1) N} - 1} & i = 1 \\ \frac{12\pi^2 \mathbf{d} e^{\pi x_2}}{1 + e^{\pi x_2}} \frac{N}{\log N} & i = 2 \\ \frac{\pi}{L'_2(\mathbf{d}, x'_3) \text{sinc}(2d)} N & i = 3 \end{cases} \quad (\text{G115})$$

where, recall, the  $L$  integrals are positive and  $0 < C < 2\pi$ .

Analyzing the individual contributions in (G113) reveals that the superdirectivity is asymptotically governed by the subset  $\mathcal{K}_3$ , which provides the dominant  $\mathcal{O}(N)$  scaling as  $N \rightarrow \infty$ . The contributions from the remaining subsets are sublinear: the subset  $\mathcal{K}_1$  exhibits an exponential decay as  $\mathcal{O}(N e^{-L_3 N})$ , while the contribution from  $\mathcal{K}_2$  converges to  $\mathcal{O}(1)$ .

Because the gaps between the bounds—stemming from subsets  $\mathcal{K}_1$  and  $\mathcal{K}_2$ —are sublinear, i.e.,  $o(N)$ , their contributions normalized by  $N$  vanish as  $N \rightarrow \infty$ . By the squeeze theorem, the bounds in (G112) are asymptotically tight, with the asymptotic scaling factor derived as

$$\tau(\mathbf{d}) = \lim_{N \rightarrow \infty} \frac{\underline{D}_{\parallel}^*(N, \mathbf{d})}{N} = \frac{\pi(1 - 2d)}{\text{sinc}(2d)} \int_0^1 \frac{1}{L'_2(\mathbf{d}, x'_3)} dx'_3 \quad (\text{G116})$$

after using  $2d' = 1 - 2d$ .

As  $d \rightarrow 1/2$ ,  $A' = -A$  approaches unity in light of (53). Consequently,  $B(\mathbf{d}, x_3)$ , bounded within  $A' < B < 1$ , is squeezed toward 1 for all  $x_3$ , as shown in Fig. 5. Evaluating the integral  $L'_2(\mathbf{d}, x'_3)$  in (91) at  $B(\mathbf{d}, x_3) = 1$  and  $d = 1/2$  causes the integral to diverge. In (G116), the reciprocal  $1/L'_2$  thus vanishes, allowing for the exchange of the limit and integration operators:

$$\lim_{d \rightarrow 1/2} \tau(\mathbf{d}) = \int_0^1 \lim_{d \rightarrow 1/2} \frac{1}{L'_2(\mathbf{d}, x'_3)} dx'_3 = \int_0^1 0 dx'_3 = 0. \quad (\text{G117})$$

As  $d \rightarrow 0$ , the scaling factor  $\tau(d)$  remains finite. Analyzing the monotonicity of  $L'_2$  via the Leibniz rule:

$$\frac{\partial}{\partial B} L'_2(d, B) = - \int_0^{\pi/2} \frac{\sin^2 \phi [3 + A - 2(1 - B) \sin^2 \phi]}{[1 + A - (1 - B) \sin^2 \phi] [2 - (1 - B) \sin^2 \phi]} d\phi. \quad (\text{G118})$$

Particularly, studying the bracketed term at the numerator, one can bound  $\sin(\cdot)$  and use the constraint  $B > -A$ , yielding

$$3 + A - 2(1 - B) \sin^2(\phi) \geq 3 + A - 2 + 2B > 1 - A \geq 0. \quad (\text{G119})$$

Hence, the derivative is nonpositive for all  $B$ . Invoking the chain rule,

$$\frac{\partial}{\partial x'_3} L'_2(d, x'_3) = \frac{\partial}{\partial B} L'_3(d, B) \cdot \frac{\partial}{\partial x'_3} B(d, x'_3), \quad (\text{G120})$$

where  $\partial B / \partial x'_3$  is positive as per (E86). Combined with (G118), this derivative means that  $L'_2(d, x'_3)$  is monotonically decreasing (its reciprocal is increasing) with  $x'_3$ . The monotonicity confirms that the dominant contribution to superdirectivity originates from the smallest eigenvalues in  $\mathcal{K}_3$ , corresponding to  $x'_3 = 1$  (see also Appendix E).

## Appendix H

To sustain the supergain as described by (95), the required condition on the loss parameter  $\rho$  relative to  $N$  and  $d$  is

$$\rho \ll d^{-1} e^{-C(d, x'_3) L'_4(d, x'_3)/2} e^{-L'_3(d, x'_3) N}, \quad (\text{H121})$$

where the integrals  $L'_i(d, x'_3)$  are defined via the kernels in (91).

By substituting the definition of  $C$  from (E57), the behavior of the first exponential term is determined by the ratio  $L'_4/L'_2$ . For  $d \rightarrow 0$ , we set  $A = 1$  in the integral  $L'_2(d, x'_3)$  according to (53), yielding

$$L'_2(0, x'_3) = \int_0^{\pi/2} \frac{2}{2 - (1 - B(0, x'_3)) \sin^2 \phi} d\phi \quad (\text{H122})$$

$$= \int_0^{\pi/2} \frac{1}{1 - \frac{1 - B(0, x'_3)}{2} \sin^2 \phi} d\phi \quad (\text{H123})$$

$$= \frac{\pi}{\sqrt{2(1 + B(0, x'_3))}}, \quad (\text{H124})$$

where  $\int_0^{\pi/2} (1 - k \sin^2 \phi)^{-1} d\phi = \frac{\pi}{2\sqrt{1-k}}$  was used. For  $L'_4(d, x'_3)$ , a direct exchange of the limit and integral leads to divergence. Instead, the denominator of the corresponding kernel

is factored as

$$L'_4(\mathbf{d}, x'_3) = \int_0^{\pi/2} \frac{2}{\alpha \sqrt{(k_1 - \sin^2 \phi)(k_2 + \sin^2 \phi)}} d\phi \quad (\text{H125})$$

with positive (in light of  $-1 < -A < B < 1$ ) parameters

$$\alpha = A + B \quad k_1 = \frac{1 + B}{A + B} \quad k_2 = \frac{1 - B}{A + B}. \quad (\text{H126})$$

Applying the change of variables  $x = \sin^2 \phi$ , such that  $d\phi = \frac{dx}{2\sqrt{x(1-x)}}$ , the integral becomes

$$L'_4(\mathbf{d}, x'_3) = \int_0^1 \frac{1}{\alpha \sqrt{x(1-x)(k_1-x)(k_2+x)}} dx \quad (\text{H127})$$

$$= \frac{2}{\alpha \sqrt{k_1(1+k_2)}} K\left(\sqrt{\frac{k_1+k_2}{k_1(1+k_2)}}\right) \quad (\text{H128})$$

$$= \frac{2}{\sqrt{(1+A)(1+B)}} K\left(\sqrt{\frac{2(A+B)}{(1+A)(1+B)}}\right), \quad (\text{H129})$$

which reduces into a scaled complete elliptic integral of the first kind  $K(\cdot)$ . Using  $K(k) \sim \ln(1/\sqrt{1-k^2})$  for  $k \rightarrow 1$  and expanding (53) as  $A \sim 1 - 2\pi^2 \mathbf{d}^2$  for  $\mathbf{d} \rightarrow 0$ ,

$$L'_4(\mathbf{d}, x'_3) \sim \sqrt{\frac{2}{1+B(0, x'_3)}} \ln\left(\frac{1}{\mathbf{d}}\right) \quad \mathbf{d} \rightarrow 0, \quad (\text{H130})$$

which converges for any  $B > -1$ , requiring in turn  $x'_3 > 0$ . (The singularity at  $x'_3 = 0$  is immaterial as the behavior within the subset  $\mathcal{K}_3$  is dominated by the smallest eigenvalues, corresponding to larger  $x'_3$ .) Combining (H124) and (H130),  $L'_4/L'_2 \sim \frac{2}{\pi} \ln(\mathbf{d}^{-1})$ . Consequently, as  $\mathbf{d} \rightarrow 0$ , the first exponential term in (H121) scales as

$$e^{-C(\mathbf{d}, x'_3)L'_4(\mathbf{d}, x'_3)/2} \sim \mathbf{d}^{\frac{4}{\pi}\Theta(\mathbf{d}, x'_3)} \quad \mathbf{d} \rightarrow 0, \quad (\text{H131})$$

where

$$\Theta(\mathbf{d}, x'_3) = \left[ \frac{N}{2} L'_1 + \left( 2 + (-1)^{\lfloor (1-2\mathbf{d})N(1-x'_3) \rfloor} \right) \frac{\pi}{4} \right]_{\text{rem } 2\pi} \quad (\text{H132})$$

subsumes the phase discontinuity in (93).

The second exponential term in (H121) depends on  $L_3(d, x'_3)$ , which is transformed similarly to (H125) as

$$L'_3(d, x'_3) = \int_0^{\pi/2} \frac{2 \sin^2 \phi}{\sqrt{(k_1 - \sin^2(\phi))(k_2 + \sin^2 \phi)}} d\phi \quad (\text{H133})$$

$$= \int_0^1 \sqrt{\frac{x}{(1-x)(k_1-x)(k_2+x)}} dx. \quad (\text{H134})$$

As  $d \rightarrow 0$ ,  $k_1 \rightarrow 1$ , creating a singularity  $1/(1-x)$  at the upper limit  $x = 1$ . This contribution is isolated by splitting the integral  $L_3(d, x'_3)$  at a cutoff  $1-a$ , such that  $0 < a < 1$ . As for the nonsingular part, on  $x \in [0, 1-a]$ ,

$$1-x \geq a \quad k_1-x \geq k_1+1+a \geq a \quad k_2+x \geq c > 0 \quad (\text{H135})$$

for some  $c > 0$ . Thus, the integrand is upper bounded by a positive constant  $C(a)$  independent of  $d$ , with corresponding integral

$$\int_0^{1-a} \sqrt{\frac{x}{(1-x)(k_1-x)(k_2+x)}} dx \leq C(a) \int_0^{1-a} dx = \mathcal{O}(1). \quad (\text{H136})$$

On the contrary, the singular contribution is evaluated as

$$I = \int_{1-a}^1 \sqrt{\frac{x}{(1-x)(k_1-x)(k_2+x)}} dx \quad (\text{H137})$$

$$= \int_0^a \sqrt{\frac{1-y}{y(\kappa_1+y)(\kappa_2-y)}} dy, \quad (\text{H138})$$

where the singular point was mapped to the origin using the inverse transformation  $y = 1-x$ . In turn,  $\kappa = k_1 - 1 = \frac{1-A}{A+B}$  and  $\kappa_2 = k_2 + 1 = \frac{1+A}{A+B}$ . Substituting

$$\kappa_1 \sim \frac{2\pi^2 d^2}{1+B}, \quad (\text{H139})$$

and noting  $\kappa_2 \sim \frac{2}{1+B}$  as  $d \rightarrow 0$ , uniformly in  $0 \leq y \leq a$  for any small  $a$ :

$$I \sim \sqrt{\frac{1+B}{2}} \int_0^a \frac{1}{\sqrt{y(y+\kappa_1)}} dy \quad (\text{H140})$$

$$= \sqrt{\frac{1+B}{2}} \left[ \ln\left(y + \frac{\kappa_1}{2} + \sqrt{y(y+\kappa_1)}\right) \right]_0^a \quad (\text{H141})$$

$$= \sqrt{\frac{1+B}{2}} \left( \ln\left(a + \frac{\kappa_1}{2} + \sqrt{a(a+\kappa_1)}\right) - \ln\left(\frac{\kappa_1}{2}\right) \right) \quad (\text{H142})$$

$$= \sqrt{2(1+B)} \left( \ln(\sqrt{a} + \sqrt{a + \kappa_1}) - \frac{1}{2} \ln \kappa_1 \right). \quad (\text{H143})$$

The above integral derives from completing the square in the denominator,  $y(y + \kappa_1) = (y + \frac{\kappa_1}{2})^2 - \frac{\kappa_1^2}{4}$ , and using [43, Eq. 2.02.14]

$$\int \frac{f'}{\sqrt{f^2 + \alpha}} dy = \ln(f + \sqrt{f^2 + \alpha}), \quad (\text{H144})$$

with  $f = y + \frac{\kappa_1}{2}$  and  $\alpha = -\frac{\kappa_1^2}{4}$ . With fixed  $a$ , since  $\kappa_1 = \mathcal{O}(d^2)$  as  $d \rightarrow 0$ , the term  $-\ln \kappa_1 = \ln(1/\kappa_1)$  dominates the expansion, resulting from (H139) into

$$I \sim \sqrt{\frac{1+B}{2}} \ln\left(\frac{1+B}{2\pi^2 d^2}\right), \quad (\text{H145})$$

which correctly leads the behavior for small  $d$  to  $\mathcal{O}(\ln(1/d))$ . Substituted into (H121), the second exponential term is

$$e^{-L'_3(d, x'_3)N} \sim \left(\frac{2\pi^2}{1+B}\right)^{N\sqrt{\frac{1+B}{2}}} d^{N\sqrt{2(1+B)}} \quad d \rightarrow 0. \quad (\text{H146})$$

Combining (H131) and (H146) into (H121), the comprehensive condition for  $\rho$  as  $d \rightarrow 0$  is, for any  $x'_3$ ,

$$\rho \ll \left(\frac{2\pi^2}{1+B}\right)^{N\sqrt{\frac{1+B}{2}}} d^{N\sqrt{2(1+B)} + \frac{4}{\pi}\Theta(d, x'_3) - 1}. \quad (\text{H147})$$

## References

- [1] Balanis, C.A.: Antenna Theory: Analysis and Design, 4th edn. Wiley-Interscience, ??? (2005)
- [2] Pizzo, A., Lozano, A.: Mutual coupling in holographic MIMO: Physical modeling and information-theoretic analysis. IEEE J. Sel. Areas Inform. Theory **6**, 111–126 (2025)
- [3] Dardari, D.: Dynamic Scattering Arrays for Simultaneous Electromagnetic Processing and Radiation in Holographic MIMO Systems (2024). <https://arxiv.org/abs/2405.16174>
- [4] Schelkunoff, S.: A mathematical theory of linear arrays. The Bell Syst. Tech. J. **22**(1), 80–107 (1943) <https://doi.org/10.1002/j.1538-7305.1943.tb01306.x>
- [5] Uzkov, A.: An approach to the problem of optimum directive antenna design. Comptes Rendus de l'Academie des Sci. de l'URSS **53**(1), 35–38 (1946) <https://doi.org/10.1002/j.1538-7305.1978.tb02104.x>

- [6] Hansen, R.C.: Fundamental limitations in antennas. *Proc. IEEE* **69**(2), 170–182 (1981) <https://doi.org/10.1109/PROC.1981.11950>
- [7] Altshuler *et al.*, E.E.: A monopole superdirective array. *IEEE Trans. Ant. Prop.* **53**(8), 2653–2661 (2005) <https://doi.org/10.1109/TAP.2005.851810>
- [8] Gilbert, E.N., Morgan, S.P.: Optimum design of directive antenna arrays subject to random variations. *The Bell Syst. Tech. J.* **34**(3), 637–663 (1955) <https://doi.org/10.1002/j.1538-7305.1955.tb01488.x>
- [9] Gustafsson, M., Nordebo, S.: Bandwidth, Q factor, and resonance models of antennas. *Progress In Electr. Research* **62**, 1–20 (2006) <https://doi.org/10.2528/PIER06033003>
- [10] Yaghjian, A.D.: Fundamentals of antenna bandwidth and quality factor. arXiv preprint arXiv:2501.03146 (2025) <https://doi.org/10.48550/arXiv.2501.03146>
- [11] Ivrlač, M.T., Nossek, J.A.: High-efficiency super-gain antenna arrays. In: *Int. ITG Workshop on Smart Antennas (WSA)*, pp. 369–374 (2010). <https://doi.org/10.1109/WSA.2010.5456400>
- [12] Ivrlač, M.T., Nossek, J.A.: Toward a circuit theory of communication. *IEEE Trans. Circuits and Systems* **57**(7), 1663–1683 (2010) <https://doi.org/10.1109/TCSI.2010.2043994>
- [13] Marzetta, T.L.: Super-directive antenna arrays: Fundamentals and new perspectives. In: *2019 53rd Asilomar Conf. Sig., Systems, and Comp.*, pp. 1–4 (2019). <https://doi.org/10.1109/IEEECONF44664.2019.9048753>
- [14] Wang, Z., Ranasinghe, K.R.R., Abreu, G.T.F., Liu, Y.: Mutual coupling in continuous aperture arrays: Physical modeling and beamforming design. arXiv preprint arXiv:2511.11225 (2025)
- [15] McMinn, B., Marzetta, T.L.: Efficient wireless power transfer considering superdirectivity in transmit and receive arrays. In: *2025 59th Asilomar Conf. Signals, Systems, and Computers*, pp. 1837–1841 (2025). <https://doi.org/10.1109/IEEECONF67917.2025.11443765>
- [16] Jeon, W., Chung, S.-Y.: Improving degrees of freedom of wireless channels using superdirectivity. In: *2015 IEEE Int. Symp. Inf. Theory (ISIT)*, pp. 2999–3003 (2015). <https://doi.org/10.1109/ISIT.2015.7283007>
- [17] Akrouf, M., Shyianov, V., Bellili, F., Mezghani, A., Heath, R.W.: Super-wideband massive MIMO. *IEEE Journal Sel. Areas Commun.* **41**(8), 2414–2430 (2023) <https://doi.org/10.1109/JSAC.2023.3288269>
- [18] Huang, L., Jin, R., Zhou, C., Li, G., Xu, L., Overvig, A., Deng, F., Chen,

- X., Lu, W., Alù, A., Miroschnichenko, A.E.: Ultrahigh-Q guided mode resonances in an all-dielectric metasurface. *Nature Commun.* **14**(1), 3433 (2023) <https://doi.org/10.1038/s41467-023-39227-5>
- [19] Fang, J., Chen, R., Sharp, D., Renzi, E.M., Manna, A., Kala, A., Mann, S.A., Yao, K., Munley, C., Rarick, H., *et al.*: Million-Q free space meta-optical resonator at near-visible wavelengths. *Nature Commun.* **15**(1), 10341 (2024) <https://doi.org/10.1038/s41467-024-54775-0>
- [20] Bikhazi, N.W., Jensen, M.A.: The relationship between antenna loss and superdirectivity in MIMO systems. *IEEE Trans. Wireless Commun.* **6**(5), 1796–1802 (2007) <https://doi.org/10.1109/TWC.2007.360381>
- [21] D’Amico, A.A., Sanguinetti, L.: Holographic MIMO communications: What is the benefit of closely spaced antennas? *IEEE Trans. Wireless Commun.* (2024)
- [22] Pizzo, A., Lozano, A.: Superdirectivity in linear holographic MIMO. In: 2024 IEEE 25th Int. Workshop Signal Process. Adv. Wireless Commun. (SPAWC), pp. 1–5 (2024). <https://doi.org/10.1109/SPAWC48557.2020.9154219>
- [23] Rhodes, D.: The optimum line source for the best mean-square approximation to a given radiation pattern. *IEEE Trans. Antennas Propag.* **11**(4), 440–446 (1963) <https://doi.org/10.1109/TAP.1963.1138075>
- [24] Hansen, T.B., Yaghjian, A.D.: *Plane-Wave Theory of Time-Domain Fields*. Wiley-IEEE Press, ??? (1999)
- [25] Taylor, T.T.: Design of line-source antennas for narrow beamwidth and low side lobes. *Trans. IRE Antennas Propag.* **3**(1), 16–28 (1955) <https://doi.org/10.1109/TPGAP.1955.5720407>
- [26] Lo, Y.T., Lee, S.W., Lee, Q.H.: Optimization of directivity and signal-to-noise ratio of an arbitrary antenna array. *Proc. IEEE* **54**(8), 1033–1045 (1966) <https://doi.org/10.1109/PROC.1966.4988>
- [27] Morris, M.L., Jensen, M.A., Wallace, J.W.: Superdirectivity in MIMO systems. *IEEE Trans. Antennas Propag.* **53**(9), 2850–2857 (2005) <https://doi.org/10.1109/TAP.2005.854530>
- [28] Gustafsson, M., Nordebo, S.: Optimal antenna currents for Q, superdirectivity, and radiation patterns using convex optimization. *IEEE Trans. Antennas Propag.* **61**(3), 1109–1118 (2013) <https://doi.org/10.1109/TAP.2012.2227656>
- [29] Orfanidis, S.J.: *Electromagnetic Waves and Antennas*. Online, ??? (2016)
- [30] Golub, G.H.: Some modified matrix eigenvalue problems. *SIAM Review* **15**(2), 318–334 (1973)

- [31] Harrington, R.: On the gain and beamwidth of directional antennas. IRE Trans. Ant. Prop. **6**(3), 219–225 (1958) <https://doi.org/10.1109/TAP.1958.1144605>
- [32] Slepian, D.: Prolate spheroidal wave functions, Fourier analysis, and uncertainty — V: The discrete case. The Bell Syst. Techn. J. **57**(5), 1371–1430 (1978) <https://doi.org/10.1002/j.1538-7305.1978.tb02104.x>
- [33] Slepian, D., Pollak, H.O.: Prolate spheroidal wave functions, Fourier analysis and uncertainty — i. The Bell System Tech. J. **40**(1), 43–63 (1961) <https://doi.org/10.1002/j.1538-7305.1961.tb03976.x>
- [34] Slepian, D.: Prolate spheroidal wave functions, Fourier analysis and uncertainty — IV: Extensions to many dimensions; generalized prolate spheroidal functions. The Bell System Techn. J. **43**(6), 3009–3057 (1964)
- [35] Slepian, D.: On bandwidth. Proc. IEEE **64**(3), 292–300 (1976) <https://doi.org/10.1109/PROC.1976.10110>
- [36] Andrei Osipov, H.X. Vladimir Rokhlin: Prolate Spheroidal Wave Functions of Order Zero. Applied Mathematical Sciences, vol. 187. Springer, ??? (2013). <https://doi.org/10.1007/978-1-4614-8259-8>
- [37] Franceschetti, M.: Wave Theory of Information. Cambridge University Press, ??? (2017). <https://doi.org/10.1017/9781139136334>
- [38] Donoho, D.L., Stark, P.B.: Uncertainty principles and signal recovery. SIAM J. Applied Math. **49**(3), 906–931 (1989) <https://doi.org/10.1137/0149053>
- [39] Slepian, D.: Some comments on Fourier analysis, uncertainty and modeling. SIAM Review **25**(3), 379–393 (1983)
- [40] Abramowitz, M., Stegun, I.A.: Handbook of Mathematical Functions. Dover Publications, New York (1972)
- [41] Bender, C.M., Orszag, S.A.: Advanced Mathematical Methods for Scientists and Engineers I: Asymptotic Methods and Perturbation Theory. Springer, New York (1999)
- [42] Do, H., Lee, N., Heath, R.W., Lozano, A.: Hybrid arrays: How many RF chains are required to prevent beam squint? IEEE Transactions on Wireless Communications **23**(9), 11708–11722 (2024) <https://doi.org/10.1109/TWC.2024.3384456>
- [43] Jeffrey, A., Zwillinger, D., Gradshteyn, I.S., Ryzhik, I.M. (eds.): Table of Integrals, Series, and Products (Seventh Edition), pp. 1–23. Academic Press, Boston (2007)